European Journal of Medicinal Chemistry 258 (2023) 115570

Contents lists available at ScienceDirect

European Journal of Medicinal Chemistry

journal homepage: www.elsevier.com/locate/ejmech

Research paper

N-aryltetrahydroisoquinoline derivatives as HA-CD44 interaction inhibitors: Design, synthesis, computational studies, and antitumor effect

Jose M. Espejo-Román [a,b,c], Belén Rubio-Ruiz [a,b,c], Meriem Chayah-Ghaddab [a,b,c], Carlos Vega-Gutierrez [a,2], Gracia García-García [a,3], Arantza Muguruza-Montero [d,1], Carmen Domene [d,e], Rosario M. Sánchez-Martín [a,b,c], Olga Cruz-López [a,c,**], Ana Conejo-García [a,c,*]

[a] Department of Medicinal and Organic Chemistry and Excellence Research Unit of Chemistry Applied to Biomedicine and the Environment, Faculty of Pharmacy, Campus Cartuja s/n, 18071, University of Granada, Granada, Spain
[b] GENYO, Centre for Genomics and Oncological Research, Pfizer/University of Granada/Andalusian Regional Government, PTS Granada, Avda. Ilustración 114, 18016, Granada, Spain
[c] Instituto de Investigación Biosanitaria de Granada (ibs.GRANADA), SAS-University of Granada, Avenida de Madrid, 15, 18012, Granada, Spain
[d] Department of Chemistry, University of Bath, Claverton Down, BA2 7AY, Bath, United Kingdom
[e] Chemistry Research Laboratory, University of Oxford, Mansfield Road, OX1 3TA, Oxford, United Kingdom

ARTICLE INFO

Keywords:
Hyaluronic acid
Cluster of differentiation 44
Tetrahydroisoquinoline
Molecular dynamics simulations
Antiproliferative effect
Three-dimensional cancer model evaluation

ABSTRACT

Hyaluronic acid (HA) plays a crucial role in tumor growth and invasion through its interaction with cluster of differentiation 44 (CD44), a non-kinase transmembrane glycoprotein, among other hyaladherins. CD44 expression is elevated in many solid tumors, and its interaction with HA is associated with cancer and angiogenesis. Despite efforts to inhibit HA-CD44 interaction, there has been limited progress in the development of small molecule inhibitors. As a contribution to this endeavour, we designed and synthesized a series of *N*-aryltetrahydroisoquinoline derivatives based on existing crystallographic data available for CD44 and HA. Hit **2e** was identified within these structures for its antiproliferative effect against two $CD44^+$ cancer cell lines, and two new analogs (**5** and **6**) were then synthesized and evaluated as CD44-HA inhibitors by applying computational and cell-based CD44 binding studies. Compound 2-(3,4,5-trimethoxybenzyl)-1,2,3,4-tetrahydroisoquinolin-5-ol (**5**) has an EC_{50} value of 0.59 μM against MDA-MB-231 cells and is effective to disrupt the integrity of cancer spheroids and reduce the viability of MDA-MB-231 cells in a dose-dependent manner. These results suggest lead **5** as a promising candidate for further investigation in cancer treatment.

1. Introduction

Cancer represents an unmet clinical need and intellectual challenge for the scientific community and is considered responsible for more than 19 million new cases worldwide and nearly 10 million deaths in 2020. Female breast cancer has surpassed lung cancer as the most frequently diagnosed cancer, with an estimated 2.3 million new cases (11.7%), followed by lung (11.4%) cancers [1].

Abbreviations: HA, hyaluronic acid; CD44, cluster of differentiation 44; CD44-HABD, CD44 HA binding domain; THIQ, tetrahydroisoquinoline.

* Corresponding author. Department of Medicinal and Organic Chemistry and Excellence Research Unit of Chemistry Applied to Biomedicine and the Environment, Faculty of Pharmacy, Campus Cartuja s/n, 18071, University of Granada, Granada, Spain.
** Corresponding author. Department of Medicinal and Organic Chemistry and Excellence Research Unit of Chemistry Applied to Biomedicine and the Environment, Faculty of Pharmacy, Campus Cartuja s/n, 18071, University of Granada, Granada, Spain.
E-mail addresses: jmespejo@ugr.es (J.M. Espejo-Román), belenrubio@ugr.es (B. Rubio-Ruiz), chayahm@ugr.es (M. Chayah-Ghaddab), carlosvg@unizar.es (C. Vega-Gutierrez), graciagg3@gmail.com (G. García-García), arantza.muguruza.montero@gmail.com (A. Muguruza-Montero), mcdn20@bath.ac.uk (C. Domene), rmsanchez@ugr.es (R.M. Sánchez-Martín), olgacl@ugr.es (O. Cruz-López), aconejo@ugr.es (A. Conejo-García).
[1] Present address: Instituto Biofisika, CSIC-UPV/EHU, 48940, Leioa, Spain.
[2] Present address: Institute for Biocomputation and Physics of Complex Systems (BIFI), University of Zaragoza, ARAID Foundation, 50018, Zaragoza, Spain.
[3] Present address: Faculty of Experimental Sciences, Universidad Francisco de Vitoria, 28223, Madrid, Spain.

https://doi.org/10.1016/j.ejmech.2023.115570
Received 15 March 2023; Received in revised form 5 June 2023; Accepted 12 June 2023
Available online 26 June 2023

The implication of hyaluronic acid (HA) in cancer biology is well documented. The expression of CD44 is upregulated in many types of malignancies in comparison to corresponding normal tissues. HA acts as a potent modulator of the tumor microenvironment *via* interaction with the cluster of differentiation 44 (CD44), creating a wide range of extracellular stimuli for tumor growth, angiogenesis, invasion, and metastasis [2]. Pathological conditions promote alternate splicing and post-translational modifications to produce diversified CD44 molecules with enhanced HA binding, leading to an increase in tumorigenicity [3,4].

Strategies to disrupt HA-CD44 interactions have been proposed as a means to target HA-induced tumorigenesis. Small HA oligosaccharides (~2.5 kDa) that compete with the endogenous HA polymer were found to inhibit downstream cell survival and proliferation pathways, stimulate apoptosis and upregulated the expression of cancer suppressor *PTEN,* and inhibit the growth of several tumors implanted as xenografts *in vivo* [5]. A natural product isolated from fungi has demonstrated potent activity as an HA antagonist (IC_{50} = 24 μM), although the molecule (fusion of a long fatty acid and trisaccharide) has not been synthesized [6]. Etoposide has been shown to inhibit the binding of MDA-MB-231 $CD44^+$ breast cancer cells to HA, disrupting key functions that drive malignancy [7].

Crystal structure and mutagenesis studies of murine and human CD44 have described essential residues in the binding of HA to CD44 [8,9]. The CD44 HA binding domain (CD44-HABD) is located in the N-terminal domain at the extracellular region of the receptor. After conducting biophysical binding assays, fragment screening, and crystallographic characterization of complexes with CD44-HABD, an inducible pocket was discovered adjacent to the HA binding groove in which small molecules were proposed to bind [9]. Iterations of fragment combination and structure-driven design established the tetrahydroisoquinoline (THIQ) pharmacophore as an attractive starting point for lead optimization. However, these THIQ derivatives were found to bind to CD44-HABD in the low millimolar range [9], and there is a vital need for new CD44 inhibitors with improved affinity, efficacy, and physicochemical properties.

Our group recently designed a novel THIQ derivative (**JE22**) that can interact with CD44-HABD. Computational studies demonstrated (Fig. 1A) that this compound binds in a similar manner to those reported in publications on the relevant crystal structures [9,10]. This finding was supported by the results of a competitive binding assay using a fluorescence-labeled HA derivative (HA-FITC) in cells. Preincubation of $CD44^+$ cells with **JE22** produces a 1.3-fold reduction in fluorescence intensity in comparison to cells incubated with HA-FITC. Furthermore, **JE22** has an EC_{50} of 8 μM against the $CD44^+$ breast cancer tumor line MDA-MB-231 [10]. To our best knowledge, this THIQ derivative is the first reported inhibitor of HA-CD44 interaction that exerts an antiproliferative effect.

The present study reports on the design, synthesis, and biological evaluation of a new series of THIQ derivatives, measuring the CD44-binding capacity, performing molecular dynamics simulations to elucidate interactions, and proposing a three-dimensional cancer model for selection of the most promising compound.

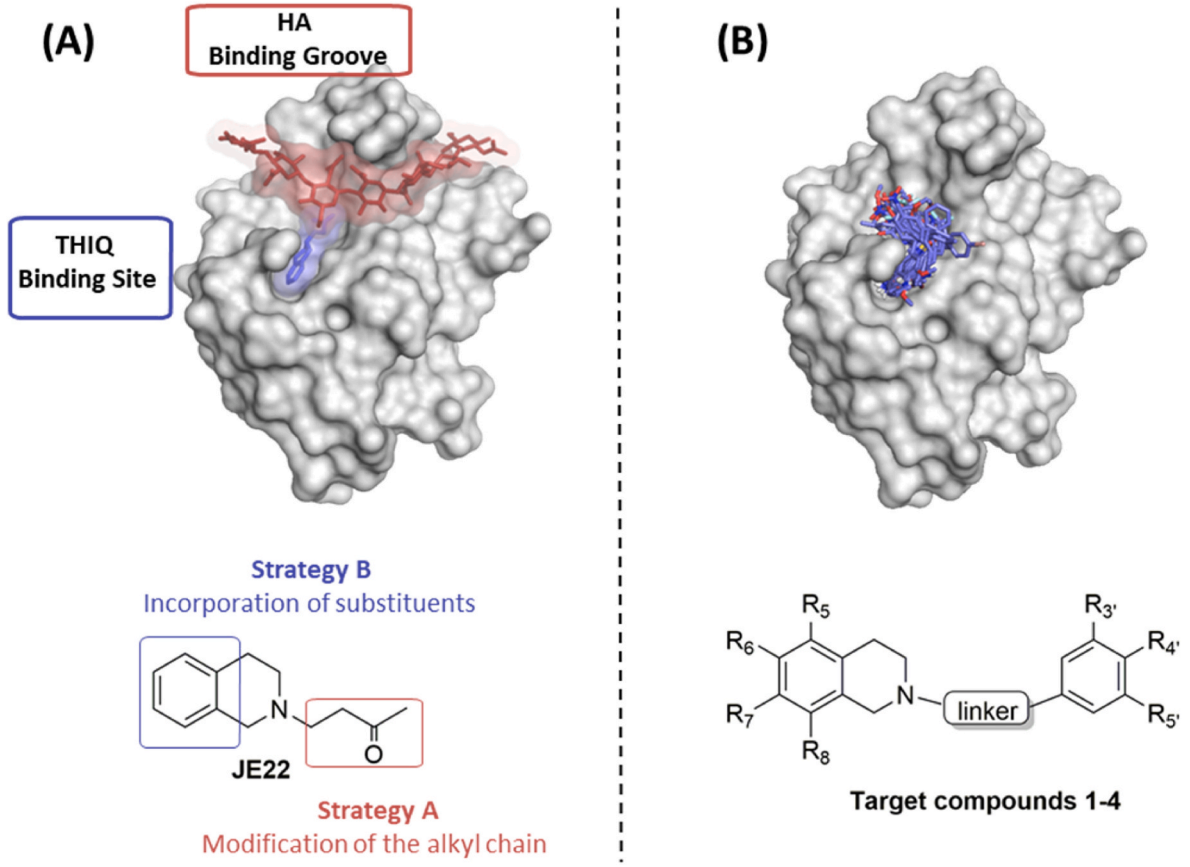

Fig. 1. (**A**) Crystallographic structure of CD44-HABD in white (PDB ID: 5BZK) highlighting the localization of HA in PDB ID: 2JCR is shown in red and **JE22** docked structure in blue. Two different strategies were followed to design target compounds based on the chemical structure of **JE22**. (**B**) Molecular docking studies reveal compounds **1**–**4** in the THIQ binding site close to the HA binding groove of CD44-HABD. The general chemical structure of compounds **1**–**4** is displayed where the linker corresponds to $–CH_2–$ or $–SO_2–$.

2. Results and discussion

2.1. Design

The previous computational studies of **JE22** (Fig. 1A) on the crystallographic structure of CD44-HABD show the close distance of the THIQ moiety to the HA binding groove. Thus, it is possible to envisage derivatives incorporating the THIQ pharmacophore that extend further into the HA binding groove. An attempt was made to achieve more selective THIQ derivatives by replacing the alkyl chain of **JE22** with aromatic rings to specifically block the binding of HA (strategy A) and adding substituents to different positions in the THIQ moiety to increase the affinity for the THIQ binding site (strategy B).

In this way, a first series of *N*-aryl THIQ derivatives was designed, comprising non-substituted THIQ (**1**), 5-aminoTHIQ (**2**), 8-aminoTHIQ (**3**), and 6,7-dimetoxyTHIQ (**4**) derivatives (Fig. 1B and Table 1). The aromatic moiety encompasses phenyl (**a**), *p*-nitrophenyl (**b** and **f**), *p*-bromophenyl (**c**), p-trifluoromethyphenyl (**d**), 3,4,5-trimetoxyphenyl (**e**), and *p*-methylphenyl (**g**).

Docking studies were carried out, and protein–ligand interactions between murine CD44-HABD and compounds **1**–**4** were analyzed at atomic level. According to these results, these compounds occupy both THIQ and HA binding sites, validating our initial hypothesis (Fig. 1B).

2.2. Chemical synthesis

The THIQ scaffold was constructed either by the reduction of 5-amino and 8-amino isoquinolines using platinum oxide (PtO) as catalyst (i, Scheme 1) [11] or by the utilization of commercially available THIQ and 6,7-dimethoxy THIQ hydrochloride. 5 and 8-amino THIQs were obtained with yields of 56% and 48%, respectively.

The target compounds (**1**–**4**) were synthesized by alkylation of the nitrogen atom of THIQ with the corresponding aryl methyl (ii, Scheme 1) or aryl sulfonyl halide (iii, Scheme 1). The reaction was carried out in dichloromethane (DCM) or absolute EtOH using triethylamine (TEA) as base.

Compounds **1a**-**1e** were synthesized following the methodology described for **1a** [12]. Reactions were carried out in DCM using two equivalents (eq.) of **9** for each eq. of corresponding aryl methyl halide to avoid the formation of the quaternary ammonium salt as a product of *N*-dialkylation of THIQ. The reaction time was 20 h, and target products were obtained with an average yield of 73%.

Sulfonyl derivatives **1f** and **1g** were obtained using 1 eq. of **9** and 1.2 eq. of sulfonyl halide in DCM as described for **1g** [13] given the non-formation of quaternary ammonium salt. TEA served as base (1.2 eq.). Reaction time was 1 h due to the higher electrophilicity of the halide. The average yield was 81%.

5-amino (**7**) and 8-amino (**8**) THIQ reagents were dissolved by using absolute EtOH in the synthesis of amino THIQ derivatives (**2a**-**2e** and **3a**-**3e**). Despite using 1 THIQ eq. per halide eq., no quaternary

Table 1
Chemical structures of target compounds.

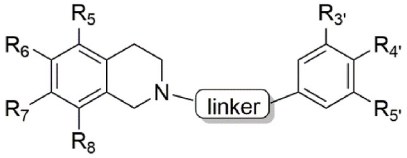

COMPOUND	R_5	R_6	R_7	R_8	LINKER	$R_{3'}$	$R_{4'}$	$R_{5'}$
1a	H	H	H	H	CH_2	H	H	H
1b	H	H	H	H	CH_2	H	NO_2	H
1c	H	H	H	H	CH_2	H	Br	H
1d	H	H	H	H	CH_2	H	CF_3	H
1e	H	H	H	H	CH_2	OCH_3	OCH_3	OCH_3
1f	H	H	H	H	SO_2	H	NO_2	H
1g	H	H	H	H	SO_2	H	CH_3	H
2a	NH_2	H	H	H	CH_2	H	H	H
2b	NH_2	H	H	H	CH_2	H	NO_2	H
2c	NH_2	H	H	H	CH_2	H	Br	H
2d	NH_2	H	H	H	CH_2	H	CF_3	H
2e	NH_2	H	H	H	CH_2	OCH_3	OCH_3	OCH_3
2f	NH_2	H	H	H	SO_2	H	NO_2	H
2g	NH_2	H	H	H	SO_2	H	CH_3	H
3a	H	H	H	NH_2	CH_2	H	H	H
3b	H	H	H	NH_2	CH_2	H	NO_2	H
3c	H	H	H	NH_2	CH_2	H	Br	H
3d	H	H	H	NH_2	CH_2	H	CF_3	H
3e	H	H	H	NH_2	CH_2	OCH_3	OCH_3	OCH_3
3f	H	H	H	NH_2	SO_2	H	NO_2	H
3g	H	H	H	NH_2	SO_2	H	CH_3	H
3h	H	H	H	*p*-NO_2PhNH	CH_2	H	NO_2	H
3i	H	H	H	*p*-CF_3PhNH	CH_2	H	CF_3	H
4a	H	OCH_3	OCH_3	H	CH_2	H	H	H
4b	H	OCH_3	OCH_3	H	CH_2	H	NO_2	H
4c	H	OCH_3	OCH_3	H	CH_2	H	Br	H
4d	H	OCH_3	OCH_3	H	CH_2	H	CF_3	H
4e	H	OCH_3	OCH_3	H	CH_2	OCH_3	OCH_3	OCH_3
4f	H	OCH_3	OCH_3	H	SO_2	H	NO_2	H
4g	H	OCH_3	OCH_3	H	SO_2	H	CH_3	H
5	OH	H	H	H	CH_2	OCH_3	OCH_3	OCH_3
6	Br	H	H	H	CH_2	OCH_3	OCH_3	OCH_3

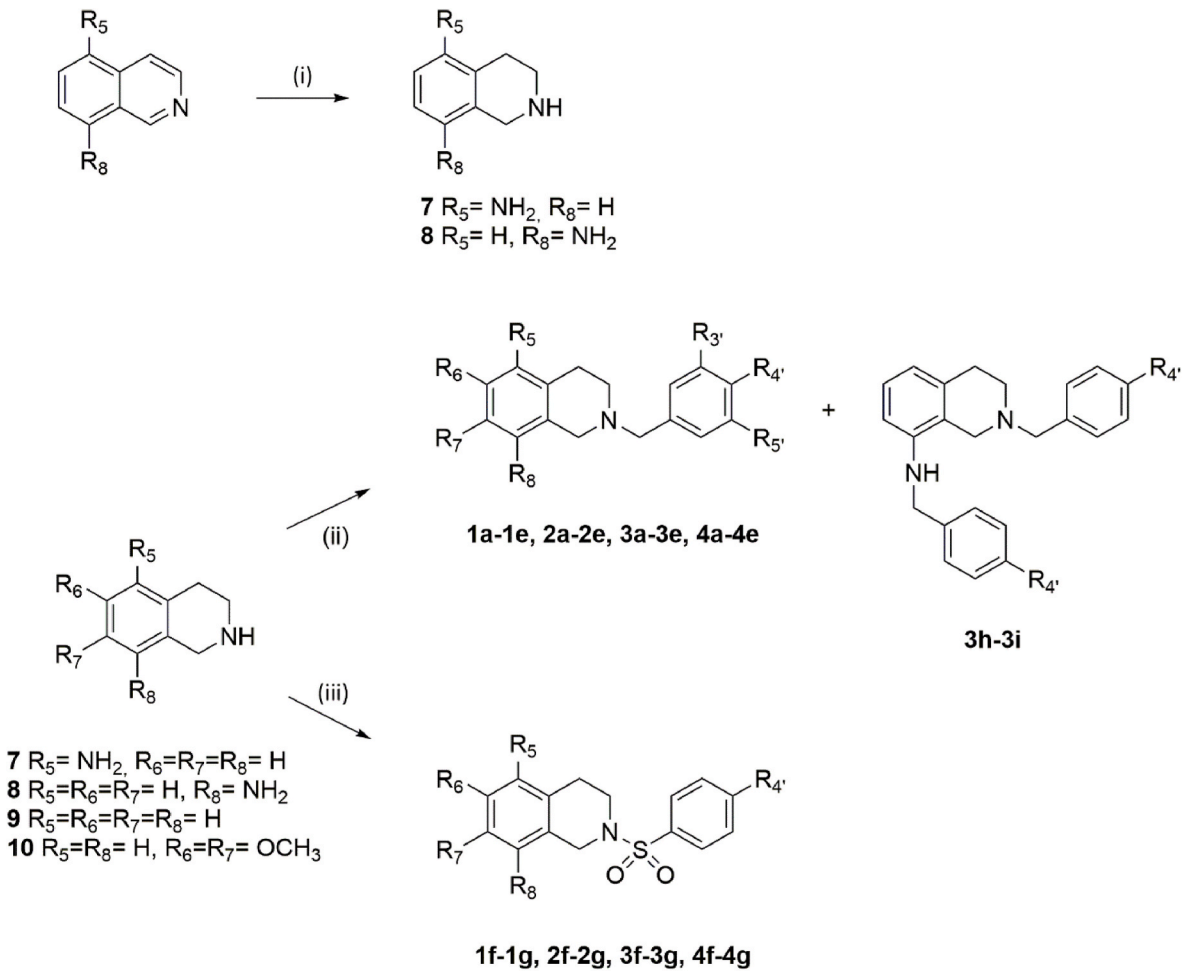

Scheme 1. Reagents and conditions: (i) H_2, PtO, AcOH, H_2SO_4 96%, rt, 55 psi, 24 h; (ii) Method a: aryl methyl halide, TEA, DCM or EtOH, 0 °C 10 min, rt 3 h or 20 h, for compounds **1a-1e**, **2a-2e**, **3a-3e**; Method b: (**10**, TEA, EtOH, rt 1 h), aryl methyl halide, TEA, rt 3.5 h, for compounds **4a-4d**, 20 h for **4e**; (iii) Method a: aryl sulfonyl halide, TEA, DCM or EtOH, 0 °C 10 min, rt 1 h or 3 h, for compounds **1f-1g**, **2f-2g** and **3f-3g**; Method b: (**10**, TEA, EtOH, rt 1 h), aryl sulfonyl halide, TEA, rt 3.5 h for **4f-4g**.

ammonium salts were isolated, and the average yield was 60% (vs. 73% for compounds **1a-1e**). Only dialkylated products at the exocyclic *N* in position 8 (**3h** and **3i**) were isolated in the reactions. The reaction time was 3 h for compounds **2a**, **2b**, **2d**, **3a** and **3c,** and 20 h for **2c**, **2e**, **3b**, **3d** and **3e**. Sulfones **f** and **g** were obtained with an average yield of 86% under the same conditions as used to obtain **2** and **3**. The reaction time for these four compounds (**2f**, **2g**, **3f** and **3g**) was 3 h.

Finally, derivatives of set **4** were obtained following a reported protocol for **4a** [14]. The free base of THIQ was obtained by the reaction of hydrochloride of 6,7-dimethoxy THIQ (**10**) (1 eq.) with 1 eq. of TEA in absolute EtOH for 1 h. Then, the corresponding halide (1 eq.) and another eq. of the base were added. The reaction time was 3.5 h with the exception of **4e** (20 h). Overall, the average yield was 63%.

2.3. In vitro antiproliferative screening

Two CD44-overexpressing tumor cell lines were initially selected: MDA-MB-231 breast adenocarcinoma and A549 epithelial lung carcinoma cell lines. Flow cytometry studies using an anti-CD44 antibody IM7 verified that both cell lines overexpress CD44, as previously reported [15–17], confirming their suitability to test the cytotoxic effect of HA-CD44 inhibitors (Fig. S1). The synthesized compounds (**1**–**4**) were then screened against the two cell lines, and their antiproliferative effects are depicted in Fig. 2 and Table S1.

All compounds generally showed similar activities in both cell lines (Fig. 2A). The most active compound, **2e,** had an EC_{50} of 2.31 μM against MDA-MB-231 cells (Fig. 2B); it has a 3,4,5-trimethoxybenzyl substituent at position 2 of THIQ, a CH_2 group as linker, and a NH_2 at position 5 of THIQ. Interestingly, all compounds bearing 3,4,5-trimethoxybenzyl (**1e**, **2e**, **3e** and **4e**) showed antiproliferative activity in MDA-MB-231 cells (≤70 μM). The amino group at position 5 is essential for the biological activity, while the non-substitution of THIQ (**1e**), a change in its position (**3e**) or introduction of the methoxy group in positions 6 and 7 (**4e**) significantly decreased their antiproliferative activity (**2e** > **1e** > **3e** > **4e**, EC_{50} MDA-MB-231 = 2.31 > 19.75>57.44 > 70.32 μM, respectively). These four compounds showed the same pattern of activity against A549 cells, although with slightly higher values (**2e** > **1e** > **3e** > **4e**, EC_{50} A549 = 3.48 > 48.19>72.42 > 77.73 μM, respectively). Compounds bearing 4-trifluoromethylbenzyl (**1d**, **2d**, **3d** and **4d**) exerted modest antiproliferative activity in both cell lines (EC_{50} MDA-MB-231 = 52.15–97.07 μM and EC_{50} A549 = 34.74–70.07 μM). Likewise, compounds with the 4-bromobenzyl moiety (**1c**, **2c**, **3c** and **4c**) showed a marked increase in activity against A549 cells (EC_{50} MDA-MB-231 = 77.07–100 μM and EC_{50} A549 = 37.90–69.90 μM). The subside product **3i** showed unexpected antiproliferative activity in both MDA-MB-231 and A549 cells (EC_{50} MDA-MB-231 = 31.49 μM and EC_{50} A549 = 36.96 μM). With regard to the linker, compounds bearing the sulfonyl group (**1f**, **1g**, **2f**, **2g**, **3f**, **3g**, **4f** and **4g**) lack antiproliferative activities (≥100 μM) except for compound **1f** (EC_{50} MDA-MB-231 = 61.77 μM) (Fig. 2 and Table S1).

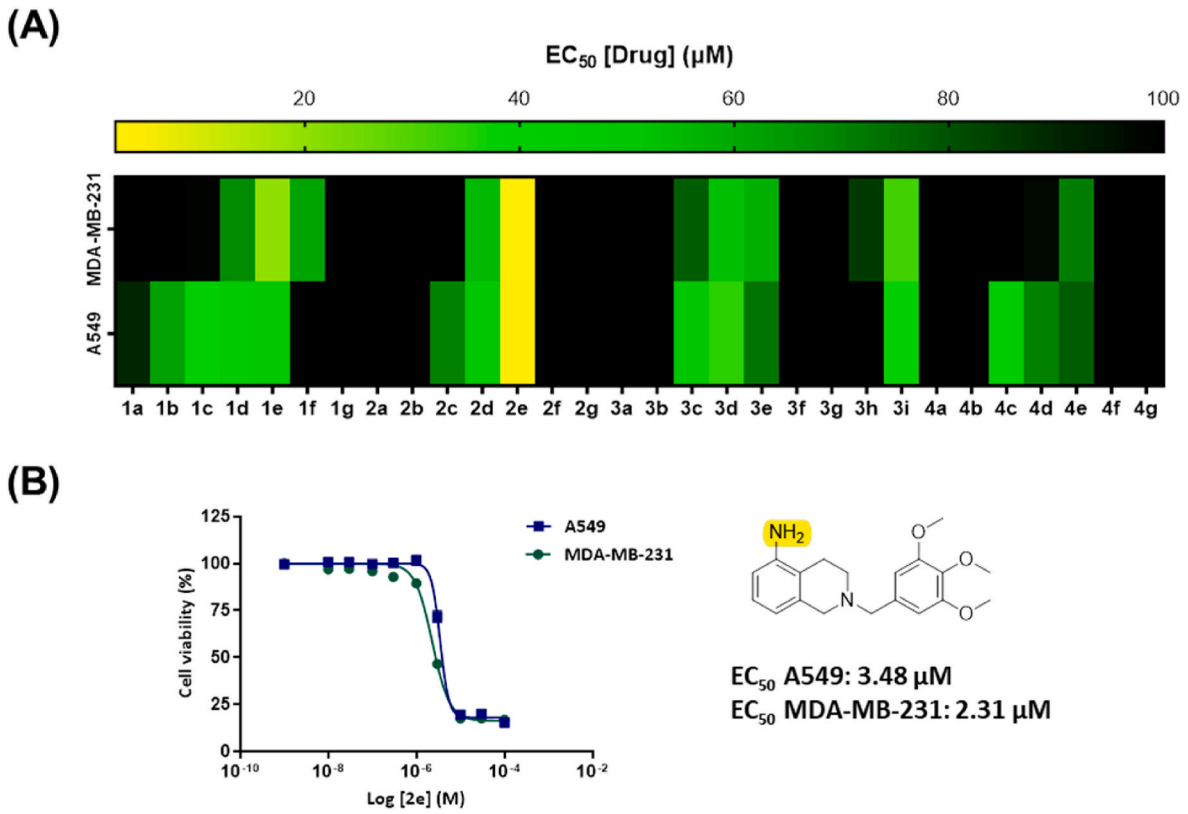

Fig. 2. *In vitro* antiproliferative screening of **1**–**4**. (**A**) Heatmap of EC_{50} values of target compounds against MDA-MB-231 and A549 cells after 5 days of treatment. Compounds with high activity are displayed in yellow and those with low activity in black. Each piece of data corresponds to the mean values of three replicas. (**B**) Dose-response curves for **2e** against MDA-MB-231 (green) and A549 (blue) cells after 5 days of treatment. Error bars: ±SD from n = 3.

2.4. Hit to lead optimization

2.4.1. Design and synthesis of compounds 5 and 6

Taking the structure of Hit **2e** as model compound, derivatives were synthesized with different substituents at position 5 of THIQ but with the trimethoxybenzyl moiety preserved at position 2. Specifically, derivatives with OH and Br substituents (**5** and **6** respectively, Scheme 2) were synthesized to study interactions of these groups in the THIQ binding pocket.

5-hydroxy THIQ acetate (**11**) was obtained by reduction of 5-hydroxyisoquinoline [18] (97%) while 5-bromo THIQ (**12**) is commercially available as hydrochloride. Both THIQ salts (1 eq.) reacted with 1 eq. of TEA in absolute EtOH for 1 h, and 1 eq. of the 3,4,5-trimetoxibenzyl chloride and 1 eq. of TEA were then added (Scheme 2). Reaction time was 20 h, and yields were 24% and 74%, respectively.

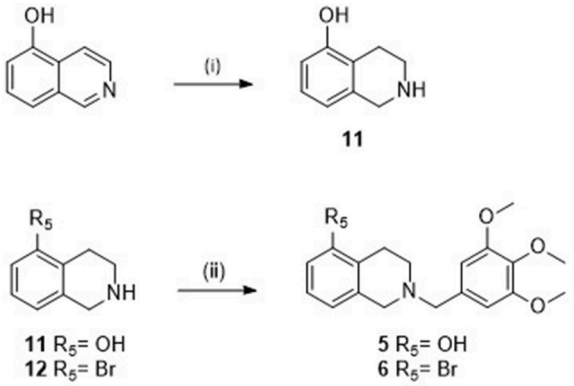

Scheme 2. Reagents and conditions: (i) H_2, PtO, AcOH, H_2SO_4 96%, rt, 55 psi, 24 h; (ii) (**11** for **5** and **12** for **6**, TEA, EtOH, rt 1 h), 3,4,5-trimetoxibenzyl chloride, TEA, rt 20 h.

2.4.2. Computational studies

Molecular modelling was performed, using compounds **5** and **6,** to gain insight into atomic interactions between compounds and glycoprotein and to compare their binding sites with that of HA. Docking study results showed that the binding of compounds **5** and **6** to CD44-HABD is similar to that of compound **2e**. The THIQ moiety of the three compounds occupied the THIQ binding site, while the trimethoxybenzyl group interacted with residues corresponding to the HA binding site (Fig. 3A). Compound **2e** shows the formation of two hydrogen bonds between Val30 of CD44-HABD and the NH_2 group at position 5 of THIQ. The oxygen of the hydroxyl group in position 5 of the THIQ moiety of compound **5** establishes a hydrogen bond with the nitrogen of the Arg155 backbone, whereas the bromo atom of compound **6** in position 5 of the THIQ moiety does not establish any of these interactions (Fig. 3B). The trimethoxybenzyl substituent of **2e** and **5** interacts in a similar manner in the HA binding groove, whereas this group is rotated in **6** (Fig. 3A).

The size of conformational space sampled is limited because the receptor is rigid during docking, and the solvent is only explicitly considered. This limitation was overcome by subjecting the docking poses selected for compounds **2e**, **5** and **6** to molecular dynamics (MD) simulations. In all five replicas of each system, comparable values to the resolution of the crystal structure were obtained for the RMSD of the backbone of the α-helical and β-sheet components of the protein, indicating that the structure of CD44-HABD is structurally stable during simulations.

Some shallow pockets close to the initial binding site could accommodate the trimethoxybenzyl group of inhibitors **2e**, **5**, and **6**. In simulations with **2e**, the ligand departed to the solution during the first 35

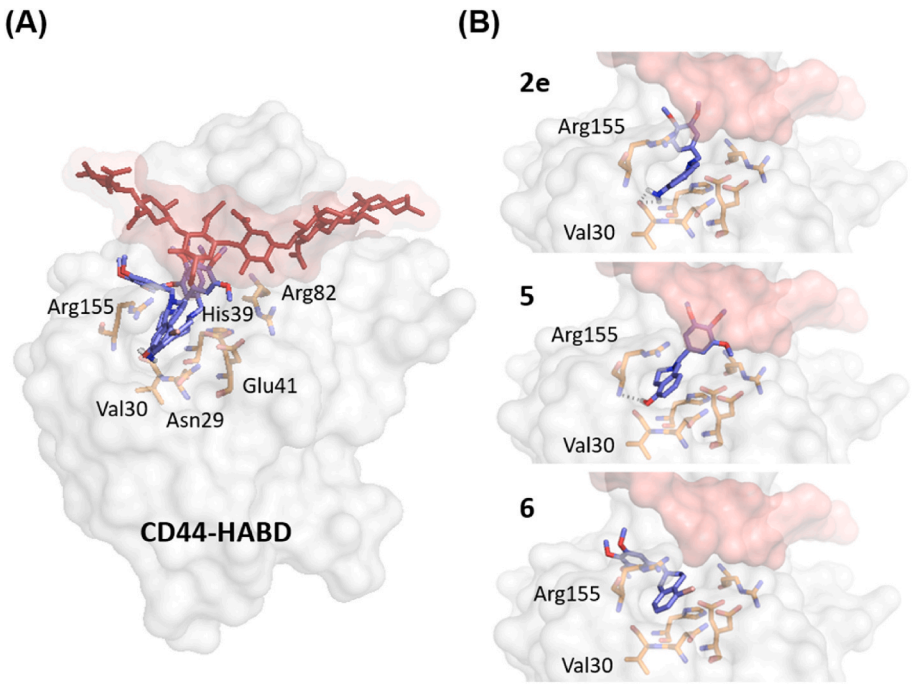

Fig. 3. Computational studies of the interactions of **2e**, **5** and **6** with CD44-HABD. (**A**) Selected poses of compounds **2e**, **5** and **6** in the THIQ binding site, expanding along the HA binding groove. (**B**) Individual selected poses for compounds **2e**, **5** and **6** indicating their interactions with key residues of CD44-HABD.

ns in all five simulations, and only in one replica returned to the protein surface, establishing transient contacts with the residues described in Table 2 and Fig. 4. In simulations with **5**, the ligand left the binding site in two of the simulations, whereas it continued to interact with the protein in a third replica, exploring different areas of its surface. In just one of the five simulations with **6**, the ligand left the protein surface and returned to the surface of CD44-HABD at 75 ns after the start of the 200-ns trajectory. Compounds **6** and **5** sometimes occupied spaces reported to be occupied by HA, especially in the vicinity of Arg155, Asn29, and Val30.

Table 2
Contacts between the protein and each ligand in a combined analysis of the trajectories from all five replicas. Contact between protein and ligand is considered when any atom of the protein is closer than 4 Å (cut-off) to any atom of the ligand. The percentage of simulation time before the observation of contact is shown. Only contacts observed after 10% of simulation time are reported. Nine residues (Arg155, Val153, Asn29, Asp156, Asn154, Gly157, Arg159, Val30, and Thr31) established interactions with all three ligands studied, and some of these were the most long-lasting interactions established during the simulations.

Compound **2e**		Compound **5**		Compound **6**	
ARG-155	21%	**ARG-155**	23%	**ARG-155**	57%
VAL-153	18%	**THR-31**	19%	**VAL-153**	47%
ASN-154	17%	**ASP-156**	19%	**ASN-29**	45%
ASN-29	17%	**ASN-29**	18%	**ASP-156**	42%
VAL-30	15%	**ASN-154**	18%	**ASN-154**	38%
GLY-157	15%	**VAL-153**	18%	**GLY-157**	35%
ASP-156	14%	**VAL-30**	18%	**ARG-159**	31%
ARG-159	13%	**GLY-157**	18%	**VAL-30**	25%
VAL-137	12%	GLU-41	16%	**THR-31**	25%
THR-31	11%	HSD-39	16%	GLU-41	21%
PRO-141	11%	ARG-50	16%	LYS-71	15%
PHE-60	11%	PHE-85	14%	ASP-27	15%
ASN-125	10%	**ARG-159**	14%	LEU-72	15%
ASP-139	10%	LEU-64	14%	SER-75	15%
LEU-111	10%	ALA-54	13%	ASN-43	14%
PHE-38	10%	ALA-53	13%	LEU-74	14%
		CYS-57	13%	GLY-107	13%
		TYR-119	11%	LYS-42	13%
		LEU-111	10%	ARG-94	12%
				Asp-68	12%
				THR-106	11%
				ARG-45	10%

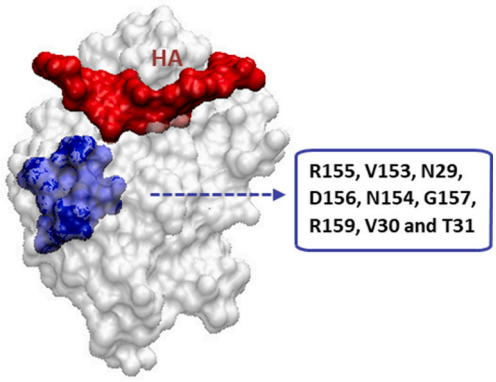

Fig. 4. Initial location of the cluster (in blue) composed by the nine residues of CD44 (PDB ID: 5BZK) (in white) found to establish interactions with **2e**, **5** and **6**. HA is shown in red. During the MD, movement of the protein loops and side chains of the residues that established contacts with the selected compounds displaced the blue cluster towards the localization of HA.

Many interactions between each ligand and the protein were shared, and the only apparent difference was in the length of time (Table 2 and Fig. 4). Overall, any of these compounds might compete with HA for the area of the protein in which HA was observed to bind crystallographically, given that the computational studies predict similar interactions between **2e, 5**, **6** and CD44-HABD.

2.4.3. Assessment of CD44-binding capacity

A competitive binding assay was performed with flow cytometry to validate the target molecules **2e**, **5** and **6** as CD44 inhibitors, applying a previously reported procedure with slight modifications [19]. HA-FITC, which has a high capacity to bind the CD44 receptor, was used as fluorescent ligand. As depicted in Fig. 5, pre-treatment of overexpressing CD44 cells MDA-MB-231 with **2e**, **5** and **6** (4 °C, 30 min, 120 μg/mL)

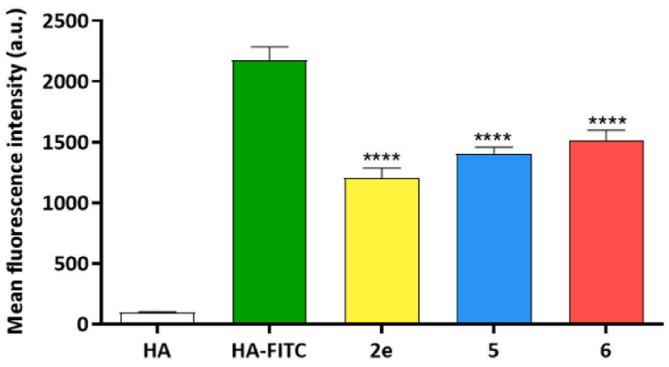

Fig. 5. HA-CD44 competitive assay. Flow cytometry analysis of MDA-MB-231 cells after treatment with **2e**, **5** and **6** (30 min, 4 °C) followed by incubation with HA-FITC (15 min, 4 °C). Cells incubated with HA-FITC and non-fluorescently-labeled HA were used as positive and negative controls, respectively. Error bars: ±SD from $n = 3$; ****$p < 0.0001$ (ANOVA).

significantly reduced the fluorescent intensity, which was 1.5-fold lower with **6** and 1.8-fold lower with **2e** in comparison to HA-FITC-incubated cells (20 μg/mL). These results suggest that these molecules displace HA-FITC binding (Fig. 5) and effectively block HA-CD44 binding.

2.4.4. Antiproliferative activity

Lead compounds **5** and **6** were only evaluated in MDA-MB-231 cells, because these had shown higher CD44 expression analysis in comparison to A549 cells, and the antiproliferative effect was also higher against MDA-MB-231 cells (Fig. S1). Both compounds were more active than **2e,** with EC_{50} values of 0.59 and 1.77 μM, respectively (Fig. 6). In this way, replacement of the amino in position 5 of THIQ by either hydroxyl or bromo substituents led to a significant increase in antiproliferative effect. Compounds **5** and **6** were 4-fold and 1.3-fold more active than **2e**, respectively.

To establish how much of the effect observed on cell viability in MDA-MB-231 cancer cells is caused by CD44 inhibition, a competitive binding experiment was conducted (Fig. S2). Cells were preincubated with the anti-CD44 antibody IM7 before treatment with the target compounds (**2e**, **5** and **6**), showing a significant decrease of the antiproliferative effect respect to cells without pretreatment (13%, 21% and 24%, respectively). This results suggest that the pretreatment with the antibody effectively blocks the CD44 cell-binding sites which prevent the ligand's recognition of epitopes indicating that the therapeutic effect of compounds **2e**, **5** and **6** is associated with CD44 recognition.

2.4.5. Three-dimensional cancer model evaluation

The use of cell cultures is of great significance in the testing of drugs, as well as in the investigation of cell biology and specific cell mechanisms. However, the widely adopted two-dimensional (2D) monolayer cell culture models do not reflect the natural cell environment, lacking essential cell-cell and cell-extracellular matrix interactions. To establish a more realistic *in vitro* model, three-dimensional (3D) cultures are preferred. One of such methods involves the formation of spheroids which is feasible in many cell lines and are thus, spheroids are widely used as models for evaluating bioactive compounds because they resemble the complex tissue environment and architecture of tumors [20]. Here, after a first screening in 2D monolayer cultures, the effect of lead compound **5** was evaluated in an established model that appears to be more clinically predictive [20]. To this end, MDA-MB-231 cells were cultured in 3D, and the resulting spheroids were treated with **5** and the negative control (DMSO) at a range of concentrations (1–100 μM) for 5 days. As shown in Fig. 7A, exposure to **5** altered the integrity of MDA-MB-231 spheroids at even the lowest concentration tested (1 μM), and a large number of dead cells detached from the spheroid core. Complete disaggregation was observed after 5 days of treatment with 100 μM. The viability of the MDA-MB-231 spheroid was also monitored (Fig. 7B), finding it to be significantly reduced by treatment with **5** in comparison to DMSO, with a dose-dependent decrease in viable cells.

3. Conclusions

A series of *N*-aryl THIQ derivatives was designed with different substituents and linked to an aromatic moiety in order to increase affinity for the THIQ binding site of CD44-HABD and/or extend into the HA binding groove. Computational studies showed that the designed resulting compounds occupy both THIQ and HA binding sites. Among these compounds, the highest antiproliferative activity is exerted by the 3,4,5-trimethoxybenzyl substituent and amino group at position 5 in compound **2e**. This antiproliferative effect was enhanced by synthesizing derivatives of the hit compound (**2e**) through replacement of the amino group at position 5 with hydroxyl (**5**) or bromine (**6**) substituents. Molecular dynamics studies suggested that these ligands can compete with HA for binding to CD44-HABD. These findings were also supported by the results of competitive binding assays with fluorescein-labeled HA, which showed that compounds **2e**, **5** and **6** effectively block HA-CD44 binding, as indicated by the significant reduction in fluorescent intensity. Compounds **5** and **6** proved to be more effective than **2e** to inhibit cell growth in MDA-MB-231 cells, observing a 4-fold increase for compound **5**. Evaluation of lead compound **5** in three-dimensional spheroids provided a more clinically predictive model of the effect of this bioactive compound in tumor environments. Exposure to lead compound **5** disrupts the integrity of MDA-MB-231 spheroids,

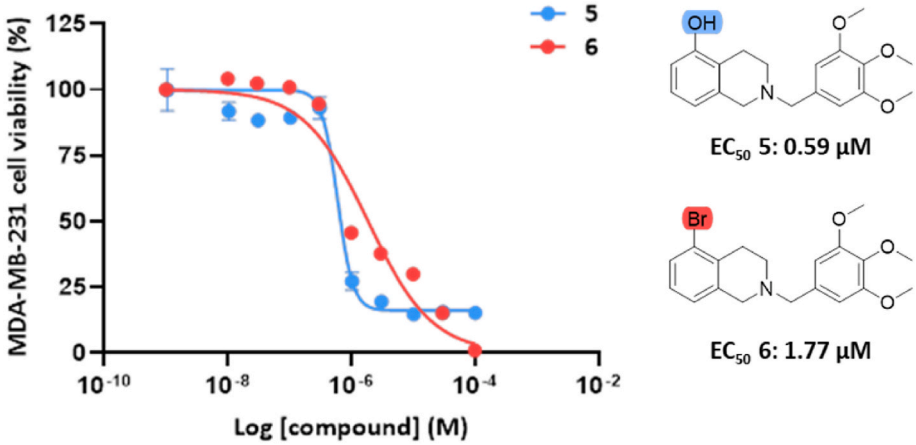

Fig. 6. Dose-response curves of target compounds **5** (blue) and **6** (red) against MDA-MB-231 cells after 5 days of treatment. Error bars: ±SD from $n = 3$.

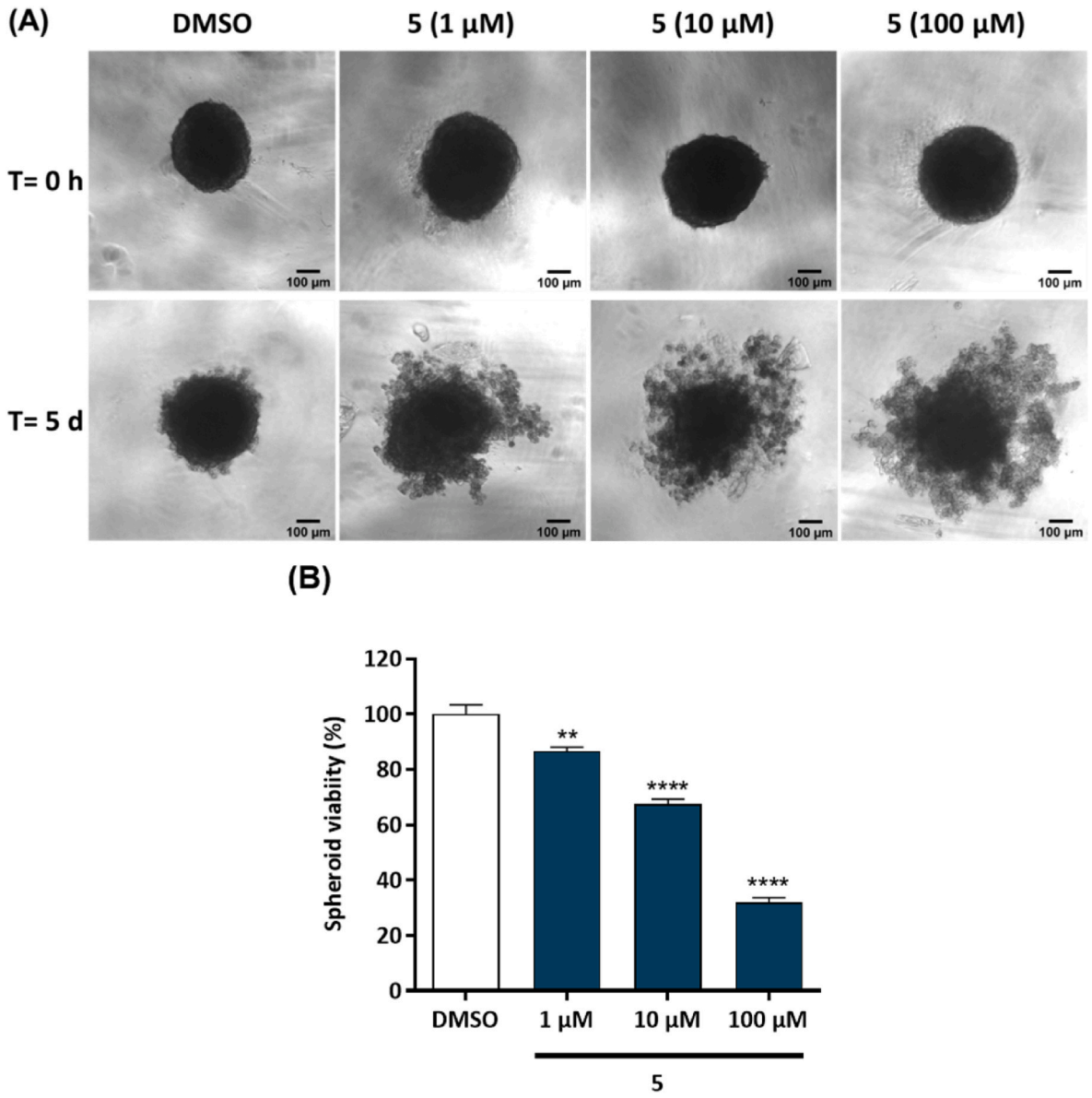

Fig. 7. MDA-MB-231 spheroid assay. (**A**) Images of spheroids treated with DMSO and **5** (1, 10, and 100 μM) at time zero (top) and at day 5 (bottom) of treatment. Scale bar: 100 μm. (**B**) Quantification of spheroid viability after 5 days of treatment with **5** (1, 10 and 100 μM). DMSO served as control. Error bars: ±SD from $n = 3$; $^{**}p < 0.01$, $^{****}p < 0.0001$ vs. control group (ANOVA).

increasing the number of dead cells detached from the spheroid core and decreasing the number of viable cells. This reduction in viability is dose-dependent, indicating the potential of lead compound **5** as a promising candidate for further investigation in cancer treatment.

4. Experimental section

4.1. Chemistry

4.1.1. General methods

Analytical thin layer chromatography (TLC) was performed using Merck Kieselgel 60 F_{254} aluminium plates and visualized by UV light (254 nm). Evaporation was carried out *in vacuo* in a Büchi rotary evaporator, and the pressure controlled by a Vacuubrand CVCII apparatus. Purifications were carried out through preparative layer chromatography or by flash column chromatography using silica gel 60 with a particle size of 0.040–0.063 nm (230–440 mesh ASTM). Melting points were taken in open capillaries on a Stuart Scientific SMP3 electrothermal melting point apparatus and are uncorrected.

NMR spectra were recorded on 500 MHz ^{1}H and 126 MHz ^{13}C NMR with a Varian Direct Drive spectrometer at ambient temperature. Chemical shifts (δ) are reported in ppm relative to the residual solvent peak. The multiplicity of each signal is given as s (singlet), d (doublet), dd (double doublet), t (triplet), q (quadruplet) and m (multiplet). J values are given in Hz. Samples were solved in deuterated solvents ($CDCl_3$, CD_3OD or DMSO). Spectra were analyzed and interpreted using MestreNova 12 software. High-resolution electrospray ionization time-of-flight (ESI-TOF) mass spectra were carried out on a Waters LCT Premier Mass Spectrometer. The samples studied were dried in a Gallencamp oven at reduced pressure with P_2O_5 inside.

All chemical reagents were supplied by Sigma-Aldrich, Thermo Fisher Scientific, VWR International Ltd and Fluorochem. Intermediates **7** [11], **8** [11], **11** [18], **1a** [12], **1g** [13] and **4a** [14], were synthesized as reported. Although target compounds **1c** [21], **1d** [22], **1f** [23], **4b** [24], **4c** [25], **4e** [26], **4f** [27], and **4g** [28] are reported, they were synthetized following the described protocols for **1a** [12], **1g** [13] and **4a** [14].

*4.1.2. General procedure for the synthesis of compounds **1a-1e***

To a solution of **9** (2 eq.) and TEA (1 eq.) in DCM (2 mL/mmol), the corresponding halide (1 eq.) was added for 10 min at 0 °C. The mixture was stirred at rt for 20 h. Then, it was washed with a saturated NaCl solution (3 × 20 mL), dried (anhydrous Na_2SO_4), filtered and concentrated under vacuum. The residue was purified by flash chromatography using hexane/ethyl acetate (AcOEt) (8:2) as eluent, except for **1e** which was purified using hexane/AcOEt (1:1).

***N*-benzyl-1,2,3,4-tetrahydroisoquinoline (1a).** Yellow oil (971 mg, 87%). **^{1}H NMR** (500 MHz, $CDCl_3$) δ 7.44 (d, J = 7.32 Hz, 2H), 7.38 (t, J = 7.34 Hz, 2H), 7.32 (d, J = 7.10 Hz, 1H), 7.20–7.10 (m, 3H), 7.02 (d, J = 7.2 Hz, 1H), 3.71 (s, 2H), 3.66 (s, 2H), 2.93 (t, J = 5.9 Hz, 2H), 2.77 (t, J = 5.9 Hz, 2H). **^{13}C NMR** (126 MHz, $CDCl_3$) δ 138.42, 134.93, 134.40, 129.09, 128.70, 128.30, 127.10, 126.61, 126.08, 125.56, 62.81, 56.14, 50.65, 29.18. **HRMS (m/z):** calcd. for $C_{16}H_{18}N$ $(M + H)^+$: 224.1361; found: 224.1437.

2-(4-nitrobencyl)-1,2,3,4-tetrahydroisoquinoline (1b). Yellow solid (1.218 g, 90%). **Mp:** 62–63 °C. **^{1}H NMR** (500 MHz, $CDCl_3$) δ 8.21 (d, J = 8.5 Hz, 2H), 7.64 (d, J = 8.5 Hz, 2H), 7.18–7.12 (m, 3H), 6.99 (d, J = 7.5 Hz, 1H), 3.85 (s, 2H), 3.72 (s, 2H), 2.97 (t, J = 5.7 Hz, 2H), 2.85 (t, J = 5.7 Hz, 2H). **^{13}C NMR** (126 MHz, $CDCl_3$) δ 147.56, 133.76, 133.55, 130.60, 129.87, 128.91, 126.73, 126.71, 126.09, 123.82, 61.45, 55.77, 50.75, 28.65. **HRMS (m/z):** calcd. for $C_{16}H_{17}N_2O_2$ $(M + H)^+$: 269.1212; found: 269.1310.

2-(4-bromobencyl)-1,2,3,4-tetrahydroisoquinoline (1c). White solid (1.520 g, 84%). **Mp:** 72–74 °C. **^{1}H NMR** (500 MHz, $CDCl_3$) δ 7.47 (d, J = 8.3 Hz, 2H), 7.32 (d, J = 8.3 Hz, 2H), 7.18–7.09 (m, 3H), 6.99 (d, J = 6.8 Hz, 1H), 3.70 (s, 2H), 3.68 (s, 2H), 2.94 (t, J = 5.8 Hz, 2H), 2.81 (t, J = 5.8 Hz, 2H). **^{13}C NMR** (126 MHz, $CDCl_3$) δ 136.53, 133.93, 133.33, 131.68, 131.05, 128.87, 126.75, 126.59, 125.99, 121.47, 61.59, 55.65, 50.49, 28.65. **HRMS (m/z):** calcd. for $C_{16}H_{17}BrN$ $(M + H)^+$: 302.0466; found: 302.0564.

2-(4-(trifluoromethyl)benzyl)-1,2,3,4-tetrahydroisoquinoline (1d). White solid (230 mg, 86%). **Mp:** 64–68 °C. **^{1}H NMR** (500 MHz, $CDCl_3$) δ 7.60 (d, J = 8.1 Hz, 2H), 7.54 (d, J = 8.1 Hz, 2H), 7.19–7.09 (m, 3H), 7.00 (d, J = 7.7 Hz, 1H), 3.75 (s, 2H), 3.65 (s, 2H), 2.92 (t, J = 5.8 Hz, 2H), 2.76 (t, J = 5.8 Hz, 2H). **^{13}C NMR** (126 MHz, $CDCl_3$) δ 142.92, 134.73, 134.35, 129.24, 128.87, 126.70, 126.37, 125.81, 125.41, 125.37, 123.07, 62.31, 56.26, 50.87, 29.26. **HRMS (m/z):** calcd. for $C_{17}H_{17}F_3N$ $(M + H)^+$: 292.1235; found: 292.1309.

2-(3,4,5-trimethoxybenzyl)-1,2,3,4-tetrahydroisoquinoline (1e). White solid (31 mg, 20%). **Mp:** 87–89 °C. **^{1}H NMR** (500 MHz, CD_3OD) δ 7.12–7.08 (m, 3H), 7.02–6.99 (m, 1H), 6.74 (s, 2H), 3.84 (s, 6H), 3.77 (s, 3H), 3.64 (s, 2H), 3.63 (s, 2H), 2.92 (t, J = 6.0 Hz, 2H), 2.77 (t, J = 6.0 Hz, 2H). **^{13}C NMR** (126 MHz, CD_3OD) δ 154.48, 138.36, 135.45, 135.15, 134.70, 129.65, 127.62, 127.47, 126.86, 107.77, 63.89, 61.10, 57.05, 56.59, 51.74, 29.60. **HRMS (m/z):** calcd. for $C_{19}H_{24}NO_3$ $(M + H)^+$: 314.1756; found: 314.1755.

*4.1.2.1. General procedure for the synthesis of compounds **1f** and **1g**.* A solution of **9** (1 eq.) and TEA (1.2 eq.) in DCM (20 mL/mmol) was cooled to 0 °C. The corresponding halide (1.2 eq.) was added to the mixture and stirred for 10 min. The reaction was then stirred for 1 h at rt. It was washed with water (1 × 10 mL) and saturated NaCl solution (3 × 10 mL), dried (anhydrous Na_2SO_4), filtered and concentrated under vacuum. The crude was purified by flash column chromatography using a hexane/AcOEt (5:1 → 1:1) solvent gradient as eluent.

2-((4-nitrophenyl)sulfonyl)-1,2,3,4-tetrahydroisoquinoline (1f). Yellow solid (194 mg, 61%). **Mp:** 180–182 °C. **^{1}H NMR** (500 MHz, $CDCl_3$) δ 8.35 (d, J = 8.7 Hz, 2H), 8.01 (d, J = 8.7 Hz, 2H), 7.19–7.13 (m, 2H), 7.10–7.01 (m, 2H), 4.35 (s, 2H), 3.47 (t, J = 5.9 Hz, 2H), 2.92 (t, J = 5.9 Hz, 2H). **^{13}C NMR** (126 MHz, $CDCl_3$) δ 150.25, 143.10, 132.83, 131.02, 129.03, 128.82, 127.21, 126.72, 126.37, 124.46, 47.51, 43.84, 28.71. **HRMS (m/z):** calcd. for $C_{15}H_{15}N_2O_4S$ $(M + H)^+$: 319.0674; found: 319.0733.

2-tosyl-1,2,3,4-tetrahydroisoquinoline (1g). White solid (312 mg, 100%). **Mp:** 148–150 °C. **^{1}H NMR** (500 MHz, $CDCl_3$) δ 7.73 (d, J = 8.2 Hz, 2H), 7.32 (d, J = 8.2 Hz, 2H), 7.16–7.11 (m, 2H), 7.09–7.06 (m, 1H), 7.04–7.01 (m, 1H), 4.25 (s, 2H), 3.36 (t, J = 5.9 Hz, 2H), 2.93 (t, J = 5.9 Hz, 2H), 2.42 (s, 3H). **^{13}C NMR** (126 MHz, $CDCl_3$) δ 143.78, 133.44, 133.20, 131.78, 129.82, 128.92, 127.87, 126.84, 126.48, 126.45, 47.67, 43.85, 29.00, 21.65. **HRMS (m/z):** calcd. for $C_{16}H_{18}NO_2S$ $(M + H)^+$: 288.0980; found: 288.1082.

*4.1.3. General procedure for the synthesis of 5-amino **(2a-2g)** and 8-amino **(3a-3i)** derivatives*

A solution of **7** or **8** (1 eq.) and TEA (1.2 eq.) in absolute EtOH (3 mL/mmol) was cooled to 0 °C. The corresponding phenylmethyl or phenylsulfonyl halide (1 eq.) was added and stirred for 10 min. Then, the reaction was stirred at rt for 3 h for compounds **2a**, **2b**, **2d**, **2f**, **2g**, **3a**, **3c**, **3f** and **3g** and 20 h for compounds **2c**, **2e**, **3b**, **3d** and **3e**. The mixture was concentrated under vacuum and the residue was purified by flash column chromatography using a hexane/AcOEt (3:1 → 1:1) solvent gradient as eluent, except compounds **2e** and **3e** which were purified using a mixture of DCM/MeOH (9.9:0.1 → 9.6:0.4) solvent gradient as eluent.

2-benzyl-1,2,3,4-tetrahydroisoquinolin-5-amine (2a). Yellow oil (53 mg, 66%). **^{1}H NMR** (500 MHz, CD_3OD) δ 7.42–7.38 (m, 2H), 7.38–7.33 (m, 2H), 7.33–7.29 (m, 1H), 6.90 (t, J = 7.7 Hz, 1H), 6.59 (d, J = 7.5 Hz, 1H), 6.40 (d, J = 7.5 Hz, 1H), 3.69 (s, 2H), 3.58 (s, 2H), 2.81 (t, J = 6.1 Hz, 2H), 2.62 (t, J = 6.1 Hz, 2H). **^{13}C NMR** (126 MHz, CD_3OD) δ 146.12, 138.26, 135.79, 130.85, 129.42, 128.56, 127.46, 120.43, 117.60, 114.41, 63.52, 57.31, 51.54, 24.98. **HRMS (m/z):** calcd. for $C_{16}H_{19}N_2$ $(M + H)^+$: 239.1548; found: 239.1533.

2-(4-nitrobenzyl)-1,2,3,4-tetrahydroisoquinolin-5-amine (2b). Yellow solid (105 mg, 55%). **Mp:** 144–146 °C. **^{1}H NMR** (500 MHz, DMSO) δ 8.22 (d, J = 8.7 Hz, 2H), 7.66 (d, J = 8.7 Hz, 2H), 6.80 (t, J = 7.7 Hz, 1H), 6.45 (d, J = 7.5 Hz, 1H), 6.21 (d, J = 7.5 Hz, 1H), 4.78 (s, 2H), 3.76 (s, 2H), 3.47 (s, 2H), 2.71 (t, J = 6.0 Hz, 2H), 2.48 (t, J = 6.0 Hz, 2H). **^{13}C NMR** (126 MHz, DMSO) δ 147.13, 146.60, 145.96, 134.79, 129.59, 125.83, 123.43, 117.99, 114.20, 111.65, 60.77, 55.88, 50.46, 24.28. **HRMS (m/z):** calcd. for $C_{16}H_{18}N_3O_2$ $(M + H)^+$: 284.1399; found: 284.1376.

2-(4-bromobenzyl)-1,2,3,4-tetrahydroisoquinolin-5-amine (2c). Yellow oil (74 mg, 69%). **^{1}H NMR** (500 MHz, CD_3OD) δ 7.49 (d, J = 8.4 Hz, 2H), 7.32 (d, J = 8.4 Hz, 2H), 6.89 (t, J = 7.7 Hz, 1H), 6.58 (d, J = 7.1 Hz, 1H), 6.39 (d, J = 7.1 Hz, 1H), 3.64 (s, 2H), 3.55 (s, 2H), 2.78 (t, J = 6.2 Hz, 2H), 2.61 (t, J = 6.2 Hz, 2H). **^{13}C NMR** (126 MHz, CD_3OD) δ 146.13, 137.83, 135.76, 132.63, 132.51, 127.47, 122.28, 120.38, 117.59, 114.41, 62.66, 57.30, 51.56, 25.04. **HRMS (m/z):** calcd. for $C_{16}H_{18}BrN_2$ $(M + H)^+$: 317.0653; found: 317.0663.

2-(4-(trifluoromethyl)benzyl)-1,2,3,4-tetrahydroisoquinolin-5-amine (2d). Yellow solid (68 mg, 66%). **Mp:** 70–72 °C. **^{1}H NMR** (500 MHz, CD_3OD) δ 7.65 (d, J = 8.2 Hz, 2H), 7.60 (d, J = 8.2 Hz, 2H), 6.89 (t, J = 7.7 Hz, 1H), 6.59 (d, J = 7.8 Hz, 1H), 6.40 (d, J = 7.8 Hz, 1H), 3.76 (s, 2H), 3.58 (s, 2H), 2.80 (t, J = 6.1 Hz, 2H), 2.62 (t, J = 6.1 Hz, 2H). **^{13}C NMR** (126 MHz, CD_3OD) δ 146.13, 143.48, 135.80, 131.13, 130.53, 127.46, 126.27, 126.25, 120.40, 117.58, 114.41, 62.84, 57.44, 51.71, 25.12. **HRMS (m/z):** calcd. for $C_{17}H_{18}F_3N_2$ $(M + H)^+$: 307.1422; found: 307.1425.

2-(3,4,5-trimethoxybenzyl)-1,2,3,4-tetrahydroisoquinolin-5-amine (2e). White solid (61 mg, 55%). **Mp:** 145–147 °C. **^{1}H NMR** (500 MHz, DMSO) δ 6.80 (t, J = 7.7 Hz, 1H), 6.65 (s, 2H), 6.44 (d, J = 7.8 Hz, 1H), 6.23 (d, J = 7.8 Hz, 1H), 4.76 (s, 2H), 3.75 (s, 6H), 3.65 (s, 3H), 3.53 (s, 2H), 3.45 (s, 2H), 2.66 (t, J = 5.7 Hz, 2H), 2.45 (t, J = 5.7 Hz, 2H). **^{13}C NMR** (126 MHz, DMSO) δ 152.80, 145.96, 136.29, 135.11, 134.35, 125.83, 118.23, 114.30, 111.61, 105.54, 61.90, 60.00, 56.07, 55.81, 50.25, 24.30. **HRMS (m/z):** calcd. for $C_{19}H_{25}N_2O_3$ $(M + H)^+$: 329.1865; found: 329.1846.

2-((4-nitrophenyl)sulfonyl)-1,2,3,4-tetrahydroisoquinolin-5-amine (2f). Orange solid (92 mg, 82%). **Mp:** 201–203 °C. **^{1}H NMR** (500

MHz, DMSO) δ 8.42 (d, J = 8.7 Hz, 2H), 8.09 (d, J = 8.7 Hz, 2H), 6.86 (t, J = 7.7 Hz, 1H), 6.48 (d, J = 7.8 Hz, 1H), 6.35 (d, J = 7.8 Hz, 1H), 4.89 (s, 2H), 4.17 (s, 2H), 3.40 (t, J = 6.0 Hz, 2H). **^{13}C NMR** (126 MHz, DMSO) δ 149.93, 146.16, 141.77, 131.48, 128.93, 126.39, 124.57, 116.66, 113.88, 112.26, 47.58, 43.49, 23.51. **HRMS (m/z):** calcd. for $C_{15}H_{16}N_3O_4S$ $(M + H)^+$: 334.0862; found: 334.0838.

2-tosyl-1,2,3,4-tetrahydroisoquinolin-5-amine (2g). White solid (84 mg, 82%). **Mp:** 182–184 °C. **^{1}H NMR** (500 MHz, $CDCl_3$) δ 7.72 (d, J = 8.2 Hz, 2H), 7.33 (d, J = 8.2 Hz, 2H), 7.03 (t, J = 7.8 Hz, 1H), 6.74 (d, J = 7.7 Hz, 1H), 6.62 (d, J = 7.7 Hz, 1H), 4.18 (s, 2H), 3.37 (t, J = 5.9 Hz, 2H), 2.74 (t, J = 5.9 Hz, 2H), 2.42 (s, 3H). **^{13}C NMR** (126 MHz, $CDCl_3$) δ 143.91, 140.93, 133.14, 133.08, 129.87, 127.94, 127.20, 120.34, 119.18, 115.32, 47.95, 43.56, 24.42, 21.67. **HRMS (m/z):** calcd. for $C_{16}H_{19}N_2O_2S$ $(M + H)^+$: 303.1167; found: 303.1156.

2-benzyl-1,2,3,4-tetrahydroisoquinolin-8-amine (3a). Yellow solid (47 mg, 58%). **Mp:** 90–92 °C. **^{1}H NMR** (500 MHz, CD_3OD) δ 7.41 (d, J = 7.4 Hz, 2H), 7.35 (t, J = 7.5 Hz, 2H), 7.28 (t, J = 7.5 Hz, 1H), 6.90 (t, J = 7.7 Hz, 1H), 6.55 (d, J = 7.9 Hz, 1H), 6.50 (d, J = 7.9 Hz, 1H), 3.75 (s, 2H), 3.50 (s, 2H), 2.82 (t, J = 5.8 Hz, 2H), 2.68 (t, J = 5.8 Hz, 2H). **^{13}C NMR** (126 MHz, CD_3OD) δ 144.75, 138.45, 135.67, 130.79, 129.41, 128.50, 127.69, 121.04, 119.73, 114.22, 63.89, 53.12, 50.73, 30.09. **HRMS (m/z):** calcd. for $C_{17}H_{18}N_2F_3$ $(M + H)^+$: 307.1402; found: 307.1422.

2-(4-nitrobenzyl)-1,2,3,4-tetrahydroisoquinolin-8-amine (3b). Yellow solid (43 mg, 45%). **Mp:** 138–140 °C. **^{1}H NMR** (500 MHz, DMSO) δ 8.21 (d, J = 8.8 Hz, 2H), 7.66 (d, J = 8.8 Hz, 2H), 6.82 (t, J = 7.7 Hz, 1H), 6.43 (d, J = 7.9 Hz, 1H), 6.33 (d, J = 7.9 Hz, 1H), 4.66 (s, 2H), 3.81 (s, 2H), 3.32 (s, 2H), 2.73 (t, J = 5.7 Hz, 2H), 2.62 (t, J = 5.7 Hz, 2H). **^{13}C NMR** (126 MHz, DMSO) δ 147.12, 146.55, 144.48, 134.14, 129.56, 126.02, 123.36, 118.86, 116.41, 111.62, 61.18, 51.78, 49.77, 29.29. **HRMS (m/z):** calcd. for $C_{16}H_{18}N_3O_2$ $(M + H)^+$: 284.1371; found: 284.1399.

2-(4-bromobenzyl)-1,2,3,4-tetrahydroisoquinolin-8-amine (3c). Yellow oil (63 mg, 60%). **^{1}H NMR** (500 MHz, CD_3OD) δ 7.50 (d, J = 8.4 Hz, 2H), 7.34 (d, J = 8.4 Hz, 2H), 6.90 (t, J = 7.7 Hz, 1H), 6.55 (d, J = 7.8 Hz, 1H), 6.50 (d, J = 7.8 Hz, 1H), 3.71 (s, 2H), 3.47 (s, 2H), 2.83 (t, J = 5.8 Hz, 2H), 2.68 (t, J = 5.8 Hz, 2H). **^{13}C NMR** (126 MHz, CD_3OD) δ 144.74, 138.03, 135.64, 132.57, 132.51, 127.71, 122.21, 121.03, 119.75, 114.25, 63.05, 53.05, 50.88, 30.16. **HRMS (m/z):** calcd. for $C_{16}H_{18}N_2Br$ $(M + H)^+$: 317.0647; found: 317.0653.

2-(4-(trifluoromethyl)benzyl)-1,2,3,4-tetrahydroisoquinolin-8-amine (3d). Yellow oil (60 mg, 58%). **^{1}H NMR** (500 MHz, CD_3OD) δ 7.65 (d, J = 8.5 Hz, 2H), 7.62 (d, J = 8.5 Hz, 2H), 6.91 (t, J = 7.7 Hz, 1H), 6.56 (d, J = 7.9 Hz, 1H), 6.51 (d, J = 7.9 Hz, 1H), 3.84 (s, 2H), 3.51 (s, 2H), 2.84 (t, J = 5.8 Hz, 2H), 2.72 (t, J = 5.8 Hz, 2H). **^{13}C NMR** (126 MHz, CD_3OD) δ 144.74, 143.58, 135.62, 131.07, 130.63, 127.73, 126.28, 125.79, 120.98, 119.76, 114.28, 63.18, 53.12, 51.06, 30.20. **HRMS (m/z):** calcd. for $C_{17}H_{18}N_2F_3$ $(M + H)^+$: 307.1402; found: 307.1422.

2-(3,4,5-trimethoxybenzyl)-1,2,3,4-tetrahydroisoquinolin-8-amine (3e). Yellow solid (20 mg, 63%). **Mp:** 127–129 °C. **^{1}H NMR** (500 MHz, DMSO) δ 6.81 (t, J = 7.7 Hz, 1H), 6.67 (s, 2H), 6.43 (d, J = 7.5 Hz, 1H), 6.32 (d, J = 7.5 Hz, 1H), 4.68 (s, 2H), 3.76 (s, 6H), 3.64 (s, 3H), 3.60 (s, 2H), 3.34 (s, 2H), 2.70 (t, J = 5.5 Hz, 2H), 2.56 (t, J = 5.5 Hz, 2H). **^{13}C NMR** (126 MHz, DMSO) δ 152.75, 144.52, 136.23, 134.42, 134.37, 125.97, 119.23, 116.45, 111.60, 105.52, 62.18, 59.94, 55.78, 51.99, 49.38, 29.34. **HRMS (m/z):** calcd. for $C_{19}H_{25}N_2O_3$ $(M + H)^+$: 329.1848; found: 329.1865.

2-((4-nitrophenyl)sulfonyl)-1,2,3,4-tetrahydroisoquinolin-8-amine (3f). Orange solid (90 mg, 80%). **Mp:** 216–218 °C. **^{1}H NMR** (500 MHz, DMSO) δ 8.44 (d, J = 9.0 Hz, 2H), 8.15 (d, J = 9.0 Hz, 2H), 6.85 (t, J = 7.7 Hz, 1H), 6.47 (d, J = 7.9 Hz, 1H), 6.33 (d, J = 7.9 Hz, 1H), 5.02 (s, 2H), 3.98 (s, 2H), 3.30 (t, J = 5.9 Hz, 2H), 2.78 (t, J = 5.9 Hz, 2H). **^{13}C NMR** (126 MHz, DMSO) δ 149.99, 144.66, 141.51, 132.98, 129.07, 126.83, 124.54, 116.39, 115.19, 112.17, 44.10, 43.14, 28.57. **HRMS (m/z):** calcd. for $C_{15}H_{16}N_3O_4S$ $(M + H)^+$: 334.0832; found: 334.0862.

2-tosyl-1,2,3,4-tetrahydroisoquinolin-8-amine (3g). White solid (126 mg, 100%). **Mp:** 260–262 °C. **^{1}H NMR** (500 MHz, DMSO) δ 7.78 (d, J = 8.3 Hz, 2H), 7.45 (d, J = 8.3 Hz, 2H), 6.85 (t, J = 7.7 Hz, 1H), 6.47 (d, J = 7.9 Hz, 1H), 6.32 (d, J = 7.9 Hz, 1H), 4.99 (s, 2H), 3.88 (s, 2H), 3.16 (t, J = 5.8 Hz, 2H), 2.76 (t, J = 5.8 Hz, 2H), 2.41 (s, 3H). **^{13}C NMR** (126 MHz, DMSO) δ 144.68, 143.49, 133.11, 132.72, 129.73, 127.63, 126.69, 116.37, 115.56, 112.12, 44.15, 43.18, 28.68, 20.98. **HRMS (m/z):** calcd. for $C_{16}H_{19}N_2O_2S$ $(M + H)^+$: 303.1167; found: 303.1167.

***N*,2-bis(4-nitrobenzyl)-1,2,3,4-tetrahydroisoquinolin-8-amine (3h).** Orange solid (14 mg, 10%). **Mp:** 170–172 °C. **^{1}H NMR** (500 MHz, $CDCl_3$) δ 8.18 (dd, J = 17.0, 8.6 Hz, 4H), 7.61 (d, J = 8.6 Hz, 2H), 7.48 (d, J = 8.6 Hz, 2H), 7.00 (t, J = 7.8 Hz, 1H), 6.61 (d, J = 7.6 Hz, 1H), 6.28 (d, J = 7.6 Hz, 1H), 4.49 (s, 2H), 3.87 (s, 2H), 3.52 (s, 2H), 2.92 (t, J = 5.6 Hz, 2H), 2.76 (t, J = 5.6 Hz, 2H). **^{13}C NMR** (126 MHz, $CDCl_3$) δ 147.45, 147.37, 147.35, 146.52, 146.46, 143.42, 135.12, 129.45, 127.71, 127.10, 124.04, 123.83, 118.96, 108.22, 62.23, 52.07, 50.03, 47.58, 29.79. **HRMS (m/z):** calcd. for $C_{23}H_{23}N_4O_4$ $(M + H)^+$: 419.1719; found: 419.1745.

***N*,2-bis(4-(trifluoromethyl)benzyl)-1,2,3,4-tetrahydroisoquinolin-8-amine (3i).** Yellow solid (14 mg, 10%). **Mp:** 123–125 °C. **^{1}H NMR** (500 MHz, CD_3OD) δ 7.64 (q, J = 8.4 Hz, 4H), 7.56 (d, J = 8.2 Hz, 2H), 7.48 (d, J = 8.2 Hz, 2H), 6.88 (t, J = 7.8 Hz, 1H), 6.44 (d, J = 7.5 Hz, 1H), 6.26 (d, J = 7.5 Hz, 1H), 4.45 (s, 2H), 3.86 (s, 2H), 3.58 (s, 2H), 2.84 (t, J = 5.8 Hz, 2H), 2.72 (t, J = 5.8 Hz, 2H). **^{13}C NMR** (126 MHz, CD_3OD) δ 146.61, 145.33, 143.63, 135.46, 131.06, 128.44, 127.75, 126.90, 126.87, 126.27, 126.23, 124.75, 124.71, 120.36, 118.68, 109.33, 63.15, 53.21, 50.79, 47.84, 30.30. **HRMS (m/z):** calcd. for $C_{25}H_{23}F_6N_2$ $(M + H)^+$: 465.1765; found: 465.1785.

*4.1.4. General procedure for the synthesis of compounds **4a-4g**, **5** and **6***

A solution of **10, 11** or **12** (1 eq.) and TEA (1 eq.) in absolute EtOH (3 mL/mmol) was stirred at rt for 1 h. Then, the corresponding halide (1 eq.) and a second eq. of TEA were added and the reaction mixture was stirred at rt for 3.5 h or 20 h for **4e**, **5** and **6**. The EtOH was removed under vacuum and the residue was dissolved in DCM and washed with a saturated NaCl solution (3 × 10 mL), dried (anhydrous Na_2SO_4), filtered and concentrated under vacuum. The reaction crude was purified by flash chromatography using a hexane/AcOEt (3:1 → 1:1) solvent gradient as eluent.

Once the reaction time has ended, for compounds **4b**, **4f** and **4g,** a suspension with a high amount of solid was observed and filtered under vacuum. This solid turned out to be the target compound. The filtering followed the same procedure described above; its purification enabled to obtain a small additional amount of the target compound. The yield of the reaction indicated for each of the compounds is the result of both fractions.

2-benzyl-6,7-dimethoxy-1,2,3,4-tetrahydroisoquinoline (4a). Yellow solid (732 mg, 59%). **Mp:** 110–112 °C. **^{1}H NMR** (500 MHz, $CDCl_3$) δ 7.41–7.31 (m, 2H), 7.34–7.29 (m, 2H), 7.28–7.22 (m, 1H), 6.58 (s, 1H), 6.47 (s, 1H), 3.82 (s, 3H), 3.79 (s, 3H), 3.67 (s, 2H), 3.53 (s, 2H), 2.86–2.77 (m, 2H), 2.75–2.66 (m, 2H). **^{13}C NMR** (126 MHz, $CDCl_3$) δ 147.45, 147.14, 138.37, 129.09, 128.25, 127.06, 126.67, 126.18, 111.40, 109.47, 62.74, 55.88, 55.86, 55.65, 50.76, 28.68. **HRMS (m/z):** calcd. for $C_{18}H_{22}NO_2$ $(M + H)^+$: 284.1572; found: 284.1654.

6,7-dimethoxy-2-(4-nitrobenzyl)-1,2,3,4-tetrahydroisoquinoline (4b). Yellow solid (60 mg, 55%). **Mp:** 116–118 °C. **^{1}H NMR** (500 MHz, $CDCl_3$) δ 8.20 (d, J = 8.6 Hz, 2H), 7.65 (d, J = 8.6 Hz, 2H), 6.61 (s, 1H), 6.47 (s, 1H), 3.86 (s, 2H), 3.84 (s, 3H), 3.80 (s, 3H), 3.65 (s, 2H), 2.95–2.80 (m, 4H). **^{13}C NMR** (126 MHz, $CDCl_3$) δ 148.06, 147.72, 147.66, 147.60, 130.01, 125.47, 124.64, 123.83, 111.55, 109.50, 61.19, 56.07, 55.20, 50.77, 28.04. **HRMS (m/z):** calcd. for $C_{18}H_{21}N_2O_4$ $(M + H)^+$: 329.1423; found: 329.1489.

2-(4-bromobenzyl)-6,7-dimethoxy-1,2,3,4-tetrahydroisoquinoline (4c). Yellow solid (263 mg, 67%). **Mp:** 108–110 °C. **^{1}H NMR** (500 MHz, $CDCl_3$) δ 7.48 (d, J = 8.3 Hz, 2H), 7.36 (d, J = 8.3 Hz, 2H), 6.60 (s, 1H), 6.46 (s, 1H), 3.83 (s, 3H), 3.80 (s, 3H), 3.77 (s, 2H), 3.67 (s, 2H),

2.95–2.85 (m, 4H). **^{13}C NMR** (126 MHz, $CDCl_3$) δ 148.13, 147.72, 132.78, 131.82, 131.38, 131.36, 131.09, 130.80, 111.51, 109.54, 56.08, 56.07, 50.32, 47.16, 29.83, 25.77. **HRMS (m/z):** calcd. for $C_{18}H_{21}BrNO_2$ $(M + H)^+$: 362.0677; found: 362.0787.

6,7-dimethoxy-2-(4-(trifluoromethyl)benzyl)-1,2,3,4-tetrahydroisoquinoline (4d). Yellow solid (54 mg, 61%). **Mp:** 106–108 °C. **^{1}H NMR** (500 MHz, $CDCl_3$) δ 7.60 (d, $J = 8.3$ Hz, 2H), 7.55 (d, $J = 8.3$ Hz, 2H), 6.61 (s, 1H), 6.48 (s, 1H), 3.84 (s, 3H), 3.81 (s, 3H), 3.78 (s, 2H), 3.60 (s, 2H), 2.90–2.84 (m, 2H), 2.83–2.77 (m, 2H). **^{13}C NMR** (126 MHz, $CDCl_3$) δ 147.88, 147.52, 142.00, 129.48, 128.38, 125.82, 125.67, 125.47, 125.43, 122.97, 111.56, 109.56, 61.80, 56.05, 55.41, 50.78, 28.34. **HRMS (m/z):** calcd. for $C_{19}H_{21}F_3NO_2$ $(M + H)^+$: 352.1446; found: 352.1536.

6,7-dimethoxy-2-(3,4,5-trimethoxybenzyl)-1,2,3,4-tetrahydroisoquinoline (4e). White solid (120 mg, 49%). **Mp:** 116–117 °C. **^{1}H NMR** (500 MHz, $CDCl_3$) δ 6.64 (s, 2H), 6.61 (s, 1H), 6.51 (s, 1H), 3.87–3.82 (m, 15H), 3.61 (s, 2H), 3.57 (s, 2H), 2.82 (t, $J = 5.7$ Hz, 2H), 2.72 (t, $J = 5.8$ Hz, 2H). **^{13}C NMR** (126 MHz, $CDCl_3$) δ 153.06, 147.64, 147.26, 136.88, 133.40, 126.16, 126.13, 126.01, 111.50, 109.61, 106.30, 62.91, 60.72, 55.97, 55.92, 55.78, 55.51, 50.63, 28.11. **HRMS (m/z):** calcd. for $C_{21}H_{27}NO_5$ $(M + H)^+$: 374.1967; found: 374.1974.

6,7-dimethoxy-2-((4-nitrophenyl)sulfonyl)-1,2,3,4-tetrahydroisoquinoline (4f). White solid (293 mg, 67%). **Mp:** 118–120 °C. **^{1}H NMR** (500 MHz, $CDCl_3$) δ 8.35 (d, $J = 8.8$ Hz, 2H), 8.01 (d, $J = 8.8$ Hz, 2H), 6.54 (s, 1H), 6.50 (s, 1H), 4.27 (s, 2H), 3.82 (s, 3H), 3.81 (s, 3H), 3.44 (t, $J = 5.9$ Hz, 2H), 2.83 (t, $J = 5.9$ Hz, 2H). **^{13}C NMR** (126 MHz, $CDCl_3$) δ 150.27, 148.26, 148.06, 143.19, 128.82, 124.77, 124.46, 122.76, 111.52, 108.95, 56.10, 56.04, 47.23, 43.89, 28.31. **HRMS (m/z):** calcd. for $C_{17}H_{19}N_2O_6S$ $(M + H)^+$: 379.0886; found: 379.0955.

6,7-dimethoxy-2-tosyl-1,2,3,4-tetrahydroisoquinoline (4g). White solid (323 mg, 86%). **Mp:** 142–144 °C. **^{1}H NMR** (500 MHz, $CDCl_3$) δ 7.71 (d, $J = 8.2$ Hz, 2H), 7.31 (d, $J = 8.2$ Hz, 2H), 6.54 (s, 1H), 6.50 (s, 1H), 4.16 (s, 2H), 3.81 (s, 3H), 3.80 (s, 3H), 3.32 (t, $J = 5.9$ Hz, 2H), 2.83 (t, $J = 5.9$ Hz, 2H), 2.41 (s, 3H). **^{13}C NMR** (126 MHz, $CDCl_3$) δ 147.97, 147.82, 143.73, 133.47, 129.78, 127.84, 125.13, 123.53, 111.45, 109.10, 56.05, 56.01, 47.35, 43.90, 28.54, 21.63. **HRMS (m/z):** calcd. for $C_{18}H_{22}NO_4S$ $(M + H)^+$: 348.1191; found: 348.1258.

2-(3,4,5-trimethoxybenzyl)-1,2,3,4-tetrahydroisoquinolin-5-ol (5). White solid (43 mg, 24%). **Mp:** 196–200 °C. **^{1}H NMR** (500 MHz, DMSO) δ 9.25 (s, 1H), 6.91 (t, $J = 7.8$ Hz, 1H), 6.66 (s, 2H), 6.61 (d, $J = 7.6$ Hz, 1H), 6.48 (d, $J = 7.6$ Hz, 1H), 3.76 (s, 6H), 3.66 (s, 3H), 3.53 (d, $J = 20.1$ Hz, 4H), 2.63 (s, 4H). **^{13}C NMR** (126 MHz, DMSO) δ 155.28, 153.26, 136.77, 136.65, 134.75, 121.61, 126.42, 117.38, 112.37, 105.99, 62.39, 60.43, 56.26, 56.14, 50.53, 24.07. **HRMS (m/z):** calcd. for $C_{19}H_{24}NO_4$ $(M + H)^+$: 330.1693; found: 330.1681.

5-bromo-2-(3,4,5-trimethoxybenzyl)-1,2,3,4-tetrahydroisoquinoline (6). White solid (174 mg, 74%). **Mp:** 88–91 °C. **^{1}H NMR** (500 MHz, $CDCl_3$) δ 7.40 (d, $J = 7.4$ Hz, 1H), 7.02–6.95 (m, 2H), 6.62 (s, 2H), 3.86 (s, 6H), 3.85 (s, 3H), 3.62 (s, 2H), 3.61 (s, 2H), 2.86 (t, $J = 5.9$ Hz, 2H), 2.76 (t, $J = 6.0$ Hz, 2H). **^{13}C NMR** (126 MHz, $CDCl_3$) δ 153.34, 137.59, 137.12, 134.45, 134.14, 130.31, 127.10, 125.89, 125.41, 105.72, 62.73, 61.00, 56.34, 56.28, 50.70, 30.43. **HRMS (m/z):** calcd. for $C_{19}H_{23}BrNO_3$ $(M + H)^+$: 392.0861; found: 392.0843.

4.2. Computational

4.2.1. Systems set up

The crystal structure of the murine CD44-HABD at 1.4 Å resolution (PDB ID: 5BZK) [9] was used as a starting point for the computational work. The binding modes of the set of compounds employed in this study were investigated by docking and subsequently, MD simulations were performed with a selection of those. The geometries of the ligands were first built with the GaussView6 software, and the ground state geometries of the neutral compounds were optimized with the GAUSSIAN package first at the Hartree-Fock level of theory using the 6-31G (d, p) basis set, and subsequently, using the B3LYP functional with the same basis set.

4.2.2. Molecular docking calculations

Docking was performed on **1**–**6** using AutoDock4.0 [29]. Crystal water molecules were removed from the PDB file. Protonation states of the protein were assigned using PropKa [30]. AutoDock4.2 was used for all docking calculations. The Lamarckian genetic algorithm and an empirical free energy function were used to search the conformational and orientation space of the inhibitors while keeping the protein structure rigid [31].

Docking parameters included an initial population of 150 randomly placed individual ligands, a maximum number of 25 million energy evaluations, a maximum of 27,000 generations, mutation and crossover rates of 0.02 and 0.80, respectively, and an elitism value of 1. AutoTors, as implemented in Autodock Tool Kit [32] was used to define the ligand torsional degrees of freedom. The grid maps representing the protein during the docking process were calculated with AutoGrid 4.2, with a grid dimension of 60 × 60 × 60 grid points, a spacing of 0.375 Å, and the center of the box was placed at the CD44-HABD binding site reported in some crystal structures (PDB entries: 4MRF, 4MRG, 4 NP2, 4 NP3, 5BZK, 5BZL, 5BZJ, 5BZM, 5BZQ, 5BZR and 5BZS). Ten independent runs were carried out for each ligand, and the docking solutions were clustered by root mean square deviation (RMSD), using a threshold of 2 Å. (Table S2). The search methods employed are stochastic and a set of optimal docked conformations is predicted. To evaluate the docking protocol used, a comparison with poses observed in some of the available crystal structures negative controls were considered. The poses resulted were analyzed using two approaches: (1) The docking results were visually inspected, (negative controls). The conformations with comparable orientations for each ligand were then selected. (2) The docking results were clustered spatially and classified considering the lowest energy for each ligand. The solutions obtained were highly clusterized which is an indication that the conformational search procedure is exhaustive enough to ensure coverage of the accessible conformational space.

4.2.3. MD simulations

The software NAMD2.14 [33] was used to perform the MD simulations of compounds **2e**, **5** and **6**. CHARMM 36 parameters were used for the protein and ions [34,35], and the transferable intermolecular potential with 3 points (TIP3P) model was used for water [36]. The charges and parameters for the ligands were compiled using the CHARMM-GUI ligand modeller interface [37] that generates the ligand force field parameters and topology files by searching for small molecules in the verified CHARMM force field library or using the CHARMM general force field (CGenFF). The protein was inserted in a water box of 90 × 90 × 90 A^3 dimensions and KCl was added up to a final concentration of 150 mM. The final systems were composed of ~45,000 atoms.

Five independent replicas were considered per system and each of them was run for 200 ns. In total, 3 μs of trajectories were analyzed after disregarding the equilibration period. The same equilibration protocol was used for all the simulations, consisting of 10,000 steps of energy minimization, followed by 10 ns of dynamics in the constant-temperature, constant-pressure (NPT) ensemble with timestep equal to 1 fs and 200 ns of dynamics in the NPT ensemble with timestep equal to 1 fs. In the course of the equilibration, restraints on the heavy atoms of the protein were gradually reduced to zero in four stages of 50 ps (1.0, 0.5 0.25 and 0.1 kcal mol for the backbone and 0.5, 0.25 0.125 and 0.05 kcal mol for the sidechain). Restraints on heavy atoms of the ligand were also released in a similar way (1.0, 0.5 0.25 and 0.1 kcal mol run for 50 ps each). Long-range electrostatic interactions were calculated with the Particle Mesh Ewald method using a grid spacing of 1.0 Å [38] and NAMD defaults for spline and κ values. A 12 Å cut-off was applied to non-bonded forces. Both electrostatics and van der Waals forces were smoothly switched off between the switching distance of 10 Å and the cut-off distance of 12 Å, using the default switching function in NAMD. The multi-time step algorithm Verlet-I/r-RESPA was used to integrate

the equations of motion [39]. The temperature was controlled at 298 K by coupling to a Langevin thermostat with a damping coefficient of 1 ps^{-1} [40]. A pressure of 1 atm was maintained by coupling the system to a Langevin piston [41], with a damping constant of 25 ps and a period of 50 ps. Analysis of the trajectories was performed using tcl scripts written in-house.

4.3. Biology

4.3.1. General methods

A NuAire NU-4750E US AutoFlow incubator was used for cell culture. Cell-based experiments were carried out in a TELSTAR BIO II Class II A laminar flow cabinet. Flow cytometry assays were performed on a FACSCanto II system using the Flowjo® 10 software for analysis. Cell viability was carried out using a GloMax-Multi Detection System to measure fluorescence. Spheroids images were acquired using an Olympus CKX53 microscope. Gibco (Thermo Fisher Scientific) was the supplier for the biological products including fetal bovine serum (FBS), trypsin-EDTA, DMEM, 1% penicillin/streptomycin, and L-glutamine. Unlabelled HA (50 KDa) and HA-FITC (50 KDa) were purchased from HAworks LLC.

4.3.2. Cell culture

Human breast carcinoma MDA-MB-231 and lung carcinoma epithelial A549 cells were provided by the Cell Bank the Center of Scientific Instrumentation of the University of Granada, and obtained from the American Type Culture Collection. These cells were cultured in DMEM with serum (10% FBS), L-glutamine (2 mM), and 1% penicillin/streptomycin and incubated in a tissue culture incubator at 37 °C, 5% CO_2 and 95% relative humidity. Cells were frequently tested negative for mycoplasma infection.

4.3.3. Flow cytometry analysis of CD44 expression

Adherent MDA-MB-231 and A549 cells were trypsinized and counted to have 10^5 cells/tube. Cells were washed twice with Staining Buffer and then incubated anti-CD44 monoclonal antibody IM7 (eBioscience) for 1 h at rt. Cells were then washed twice and incubated with a secondary Rabbit anti-Mouse IgG (H + L) antibody Alexa Fluor™ 488 (AB_2534106, Thermo Fisher Scientific) for 30 min at rt. Cells were washed twice and analyzed by flow cytometry using FACSCanto II (Becton Dickinson & Co., Franklin Lakes, NJ, USA) and Flowjo® 10 software (Becton Dickinson & Co., Franklin Lakes, NJ, USA). Untreated cells together with cells treated with Mouse IgG1 isotype control (AB_2532935, Thermo Fisher Scientific) and cells treated only with IgG secondary antibody were used as negative controls.

4.3.4. Cell viability assays

Target compounds were dissolved in DMSO and stored at −20 °C. For each experiment, the stock solution (100 mM) was further diluted in culture media to obtain the desired concentrations. MDA-MB-231 (2,000 cells/well) and A549 cells (1,500 cells/well) were seeded in a 96-well plate format and incubated for 24 h before treatment. Each well was then replaced with fresh media, containing target compounds (0.01–100 μM) and incubated for 5 days. Untreated cells (DMSO, 0.1% *v/v*) were used as control to detect any undesirable effects of culture conditions on cell viability. Each condition was performed in triplicates. PrestoBlue™ cell viability reagent (10% *v/v*) was added to each well and the plate incubated for 120 min. Fluorescence emission was detected using a GloMax-Multi Detection System (excitation filter at 540 nm and emission filter at 590 nm). All conditions were normalized to the untreated cells (100%) and the curve fitted using GraphPad Prism using a sigmoidal variable slope curve. The EC_{50} value is expressed as the mean ± SD of three independent experiments.

The cell viability of compounds **2e**, **5** and **6** was also determined preincubating with anti-CD44 antibody IM7 (eBioscience) for 30 min at rt.

4.3.5. HA-FITC binding assay

Adherent MDA-MB-231 cells were trypsinized, counted, and diluted in DMEM in order to have 5×10^4 cells/eppendorf tube. Cells were centrifuged for 5 min, and pellets were resuspended in DMEM media containing compounds **2e**, **5** or **6** (120 μg/mL). Samples were incubated at 4 °C for 30 min. Then, cells were centrifuged for 5 min, and pellets were resuspended in DMEM media containing HA-FITC (20 μg/mL) and incubated at 4 °C for 15 min. Cells incubated with unlabelled HA were used as the negative control, whereas cells incubated with HA-FITC served as the positive control. After incubation, cells were centrifuged and resuspended in PBS, and samples were analyzed by flow cytometry (FACSCanto II). Flowjo® 10 software was used for data analysis. Results are expressed as the MFI ±SD of three independent experiments.

4.3.6. Statistical analysis

One-way ANOVA analysis and Student's *t*-test was performed using the GraphPad 8.0 software.

4.3.7. Spheroids assay

MDA-MB-231 spheroids were generated using the centrifugal forced-aggregation technique. Briefly, cells were separated from the flasks using trypsin, washed with PBS, resuspended, and counted. 5,000 cells per well/100 μL were seeded in ultra-low attachment round bottom 96-well plates. Plates were centrifuged at 290 g for 3 min and placed in a tissue culture incubator. After 24 h, 50 μL of complete medium containing 18 μg/mL of collagen was added to each well to get the optimal concentration of collagen (6 μg/mL). Then, plates were centrifuged at 100 g for 3 min and placed back for 3 days in the incubator until the complete formation of spheroids. On day 5, spheroids were treated with **5** at various concentrations (1 μM, 10 μM and 100 μM), and DMSO (0.1% *v/v*) was used as vehicle control. Each condition was performed in three biological replicas.

On day 10 (5 days after treatment), a cell viability assay of 3D spheroids was performed. PrestoBlue™ cell viability reagent (10% *v/v*) was added to each well and the plates were incubated for 6 h. Following this, the plates were centrifuged at 290 g for 3 min and fluorescence emission was determined using a GloMax-Multi Detection System (excitation filter at 540 nm and emission filter at 590 nm). The data were exported to Microsoft Excel and GraphPad Prism for analysis.

In addition, spheroids were imaged at time zero and after 5 days of treatment using an Olympus CKX53 microscope (4 × objective magnification) and processed with ImageJ® software.

Funding

This research was funded by the Consejería de Universidad, Investigación e Innovación of the Junta de Andalucía and FEDER, Una manera de hacer Europa (P18-RT-1679, PT18-TP-4160, B-FQM-475-UGR18 and PAIDI-TC-PVT-PSETC-2.0.), the Research Results Transfer Office (OTRI) of the University of Granada (PR/17/006), the Spanish Ministry of Economy and Competitiveness (PID2019.110987RB.I00 and PID2021.128109OB.I00) and the Health Institute Carlos III (DTS18/00121). C.D. thanks HECBioSim, the UK High End Computing Consortium for Biomolecular Simulation (hecbiosim.ac.uk), which is supported by the EPSRC (EP/L000253/1) for awarding computing time in Jade, a UK Tier-2 resource. B.R.-R. gratefully acknowledges funding from the European Union's Horizon 2020 Research and Innovation Program under Marie Sklodowska-Curie Grant Agreement no. 754446 and UGR Research and Knowledge Transfer Fund—Athenea3i. J.M.E.-R. thanks the Spanish Ministry of Education for a studentship (FPU 16/02061). A.M.-M. gratefully acknowledges funding from the HPC-Europa3 Transnational Access programme supported by the European Commission H2020 Research & Innovation GA # 730897 (application number HPC17ARM6V). Funding for open access charge: Universidad de Granada / CBUA.

Declaration of competing interest

The authors declare that they have no known competing financial interests or personal relationships that could have appeared to influence the work reported in this paper.

Data availability

Data will be made available on request.

Appendix A. Supplementary data

Supplementary data to this article can be found online at https://doi.org/10.1016/j.ejmech.2023.115570.

References

[1] H. Sung, J. Ferlay, R.L. Siegel, M. Laversanne, I. Soerjomataram, A. Jemal, F. Bray, Global cancer statistics 2020: GLOBOCAN estimates of incidence and mortality worldwide for 36 cancers in 185 countries, CA, A Cancer J. Clin. 71 (2021) 209–249, https://doi.org/10.3322/caac.21660.

[2] T. Chanmee, P. Ontong, N. Itano, Hyaluronan: a modulator of the tumor microenvironment, Cancer Lett. 375 (2016) 20–30, https://doi.org/10.1016/j.canlet.2016.02.031.

[3] S. Misra, P. Heldin, V.C. Hascall, N.K. Karamanos, S.S. Skandalis, R.R. Markwald, S. Ghatak, Hyaluronan-CD44 interactions as potential targets for cancer therapy: targeting CD44 variants in tumors, FEBS J. 278 (2011) 1429–1443, https://doi.org/10.1111/j.1742-4658.2011.08071.x.

[4] S.S. Skandalis, T.T. Karalis, A. Chatzopoulos, N.K. Karamanos, Hyaluronan-CD44 axis orchestrates cancer stem cell functions, Cell. Signal. 63 (2019), 109377, https://doi.org/10.1016/j.cellsig.2019.109377.

[5] M.G. Slomiany, L. Dai, L.B. Tolliver, G.D. Grass, Y. Zeng, B.P. Toole, Inhibition of functional hyaluronan-CD44 interactions in CD133-positive primary human ovarian carcinoma cells by small hyaluronan oligosaccharides, Clin. Cancer Res. 15 (2009) 7593–7601, https://doi.org/10.1158/1078-0432.CCR-09-2317.

[6] Y. Hirota-Takahata, H. Harada, I. Tanaka, T. Nakata, M. Nakajima, M. Takahashi, F-19848 A, a novel inhibitor of hyaluronic acid binding to cellular receptor CD44, J. Antibiot. 60 (2007) 633–639, https://doi.org/10.1038/ja.2007.81.

[7] C. Aguirre-Alvarado, A. Segura-Cabrera, I. Velázquez-Quesada, M.A. Hernández-Esquivel, C.A. García-Pérez, S.L. Guerrero-Rodríguez, A.J. Ruiz-Moreno, A. Rodríguez-Moreno, S.M. Pérez-Tapia, M.A. Velasco-Velázquez, Virtual screening-driven repositioning of etoposide as CD44 antagonist in breast cancer cells, Oncotarget 7 (2016) 23772–23784, https://doi.org/10.18632/oncotarget.8180.

[8] S. Banerji, A.J. Wright, M. Noble, D.J. Mahoney, I.D. Campbell, A.J. Day, D. G. Jackson, Structures of the Cd44-hyaluronan complex provide insight into a fundamental carbohydrate-protein interaction, Nat. Struct. Mol. Biol. 14 (2007) 234–239, https://doi.org/10.1038/nsmb1201.

[9] L.-K. Liu, B.C. Finzel, Fragment-based identification of an inducible binding site on cell surface receptor CD44 for the design of protein–carbohydrate interaction inhibitors, J. Med. Chem. 57 (2014) 2714–2725, https://doi.org/10.1021/jm5000276.

[10] J.M. Espejo-Román, B. Rubio-Ruiz, V. Cano-Cortés, O. Cruz-López, S. Gonzalez-Resines, C. Domene, A. Conejo-García, R.M. Sánchez-Martín, Selective anticancer therapy based on a HA-CD44 interaction inhibitor loaded on polymeric nanoparticles, Pharmaceutics 14 (2022) 788, https://doi.org/10.3390/pharmaceutics14040788.

[11] J.D. Harling, B.S. Orlek, M. Thompson, Substituted Benzamide Derivatives and Their Use as Anticonvulsants, WO1997048683A1, 1997.

[12] K.M. Jones, P. Karier, M. Klussmann, C1-Substituted N-alkyl tetrahydroisoquinoline derivatives through V-catalyzed oxidative coupling, ChemCatChem 4 (2012) 51–54, https://doi.org/10.1002/cctc.201100324.

[13] C. Yan, Y. Liu, Q. Wang, Mild and highly efficient metal-free oxidative α-cyanation of N-acyl/sulfonyl tetrahydroisoquinolines, RSC Adv. 4 (2014) 60075–60078, https://doi.org/10.1039/C4RA12922A.

[14] M. Lüthy, V. Darmency, P. Renaud, Modified B-alkylcatecholboranes as radical precursors, Eur. J. Org Chem. 2011 (2011) 547–552, https://doi.org/10.1002/ejoc.201001120.

[15] E. Olsson, G. Honeth, P.-O. Bendahl, L.H. Saal, S. Gruvberger-Saal, M. Ringnér, J. Vallon-Christersson, G. Jönsson, K. Holm, K. Lövgren, M. Fernö, D. Grabau, Å. Borg, C. Hegardt, CD44 isoforms are heterogeneously expressed in breast cancer and correlate with tumor subtypes and cancer stem cell markers, BMC Cancer 11 (2011) 418, https://doi.org/10.1186/1471-2407-11-418.

[16] C. Sheridan, H. Kishimoto, R.K. Fuchs, S. Mehrotra, P. Bhat-Nakshatri, C.H. Turner, R. Goulet, S. Badve, H. Nakshatri, CD44+/CD24-breast cancer cells exhibit enhanced invasive properties: an early step necessary for metastasis, Breast Cancer Res. 8 (2006) R59, https://doi.org/10.1186/bcr1610.

[17] N. Zakaria, N.M. Yusoff, Z. Zakaria, M.N. Lim, P.J.N. Baharuddin, K.S. Fakiruddin, B. Yahaya, Human non-small cell lung cancer expresses putative cancer stem cell markers and exhibits the transcriptomic profile of multipotent cells, BMC Cancer 15 (2015) 84, https://doi.org/10.1186/s12885-015-1086-3.

[18] M. Azimioara, C. Cow, R. Epple, S. Jiang, G. Lelais, D. Mutnick, B. Wu, Compounds and Compositions as Modulators of Gpr119 Activity, WO2009105717A1, 2009.

[19] D.S. Bhattacharya, D. Svechkarev, J.J. Souchek, T.K. Hill, M.A. Taylor, A. Natarajan, A.M. Mohs, Impact of structurally modifying hyaluronic acid on CD44 interaction, J. Mater. Chem. B 5 (2017) 8183–8192, https://doi.org/10.1039/C7TB01895A.

[20] K. Białkowska, P. Komorowski, M. Bryszewska, K. Miłowska, Spheroids as a type of three-dimensional cell cultures—examples of methods of preparation and the most important application, Int. J. Mol. Sci. 21 (2020) 6225, https://doi.org/10.3390/ijms21176225.

[21] G. Oss, S.D. de Vos, K.N.H. Luc, J.B. Harper, T.V. Nguyen, Tropylium-promoted oxidative functionalization of tetrahydroisoquinolines, J. Org. Chem. 83 (2018) 1000–1010, https://doi.org/10.1021/acs.joc.7b02584.

[22] S. Schnatterer, M. Maier, F. Petry, W. Knauf, K. Seeger, Pesticidal Substituted Piperidines, 2006, WO2006087162.

[23] S.P. Miller, Y.-L. Zhong, Z. Liu, M. Simeone, N. Yasuda, J. Limanto, Z. Chen, J. Lynch, V. Capodanno, Practical and cost-effective manufacturing route for the synthesis of a β-lactamase inhibitor, Org. Lett. 16 (2014) 174–177, https://doi.org/10.1021/ol4031606.

[24] F. Antoni, M. Bause, M. Scholler, S. Bauer, S.A. Stark, S.M. Jackson, I. Manolaridis, K.P. Locher, B. König, A. Buschauer, G. Bernhardt, Tariquidar-related triazoles as potent, selective and stable inhibitors of ABCG2 (BCRP), Eur. J. Med. Chem. 191 (2020), 112133, https://doi.org/10.1016/j.ejmech.2020.112133.

[25] Y. Zhou, J. Wang, Q. Jiang, Tetrahydroisoquinoline Derivative with Antifungal Activity and its Preparation Method, 2003, p. CN1412182A.

[26] W. Dohle, M.P. Leese, F.L. Jourdan, C.J. Chapman, E. Hamel, E. Ferrandis, B.V. L. Potter, Optimisation of tetrahydroisoquinoline-based chimeric microtubule disruptors, ChemMedChem 9 (2014) 1783–1793, https://doi.org/10.1002/cmdc.201402025.

[27] H.P. Kim, H. Yu, H. Kim, S.-H. Kim, D. Lee, DDQ-promoted mild and efficient metal-free oxidative α-cyanation of N-Acyl/Sulfonyl 1,2,3,4-tetrahydroisoquinolines, Molecules 23 (2018) 3223, https://doi.org/10.3390/molecules23123223.

[28] H. Senboku, K. Nakahara, T. Fukuhara, S. Hara, Hg cathode-free electrochemical detosylation of N,N-disubstituted p-toluenesulfonamides: mild, efficient, and selective removal of N-tosyl group, Tetrahedron Lett. 51 (2010) 435–438, https://doi.org/10.1016/j.tetlet.2009.11.056.

[29] G.M. Morris, D.S. Goodsell, R.S. Halliday, R. Huey, W.E. Hart, R.K. Belew, A. J. Olson, Automated docking using a Lamarckian genetic algorithm and an empirical binding free energy function, J. Comput. Chem. 19 (1998) 1639–1662, https://doi.org/10.1002/(SICI)1096-987X(19981115)19:14<1639::AID-JCC10>3.0.CO;2-B.

[30] M.H.M. Olsson, C.R. Søndergaard, M. Rostkowski, J.H. Jensen, PROPKA3: consistent treatment of internal and surface residues in empirical pKa predictions, J. Chem. Theor. Comput. 7 (2011) 525–537, https://doi.org/10.1021/ct100578z.

[31] R. Huey, G.M. Morris, A.J. Olson, D.S. Goodsell, A semiempirical free energy force field with charge-based desolvation, J. Comput. Chem. 28 (2007) 1145–1152, https://doi.org/10.1002/jcc.20634.

[32] G.M. Morris, R. Huey, W. Lindstrom, M.F. Sanner, R.K. Belew, D.S. Goodsell, A. J. Olson, AutoDock4 and AutoDockTools4: automated docking with selective receptor flexibility, J. Comput. Chem. 30 (2009) 2785–2791, https://doi.org/10.1002/jcc.21256.

[33] W. Humphrey, A. Dalke, K. Schulten, VMD: visual molecular dynamics, J. Mol. Graph. 14 (1996) 33–38, https://doi.org/10.1016/0263-7855(96)00018-5.

[34] J. Huang, A.D. MacKerell, CHARMM36 all-atom additive protein force field: validation based on comparison to NMR data, J. Comput. Chem. 34 (2013) 2135–2145, https://doi.org/10.1002/jcc.23354.

[35] A.D. MacKerell, D. Bashford, M. Bellott, R.L. Dunbrack, J.D. Evanseck, M.J. Field, S. Fischer, J. Gao, H. Guo, S. Ha, D. Joseph-McCarthy, L. Kuchnir, K. Kuczera, F.T. K. Lau, C. Mattos, S. Michnick, T. Ngo, D.T. Nguyen, B. Prodhom, W.E. Reiher, B. Roux, M. Schlenkrich, J.C. Smith, R. Stote, J. Straub, M. Watanabe, J. Wiórkiewicz-Kuczera, D. Yin, M. Karplus, All-atom empirical potential for molecular modeling and dynamics studies of proteins, J. Phys. Chem. B 102 (1998) 3586–3616, https://doi.org/10.1021/jp973084f.

[36] W.L. Jorgensen, J. Chandrasekhar, J.D. Madura, R.W. Impey, M.L. Klein, Comparison of simple potential functions for simulating liquid water, J. Chem. Phys. 79 (1983) 926–935, https://doi.org/10.1063/1.445869.

[37] S. Kim, J. Lee, S. Jo, C.L. Brooks III, H.S. Lee, W. Im, CHARMM-GUI ligand reader and modeler for CHARMM force field generation of small molecules, J. Comput. Chem. 38 (2017) 1879–1886, https://doi.org/10.1002/jcc.24829.

[38] T. Darden, D. York, L. Pedersen, Particle mesh Ewald: an N·log(N) method for Ewald sums in large systems, J. Chem. Phys. 98 (1993) 10089–10092, https://doi.org/10.1063/1.464397.

[39] L. Verlet, Computer "experiments" on classical fluids. I. Thermodynamical properties of Lennard-Jones molecules, Phys. Rev. 159 (1967) 98–103, https://doi.org/10.1103/PhysRev.159.98.

[40] E.A. Koopman, C.P. Lowe, Advantages of a Lowe-Andersen thermostat in molecular dynamics simulations, J. Chem. Phys. 124 (2006), 204103, https://doi.org/10.1063/1.2198824.

[41] S.E. Feller, Y. Zhang, R.W. Pastor, B.R. Brooks, Constant pressure molecular dynamics simulation: the Langevin piston method, J. Chem. Phys. 103 (1995) 4613–4621, https://doi.org/10.1063/1.470648.